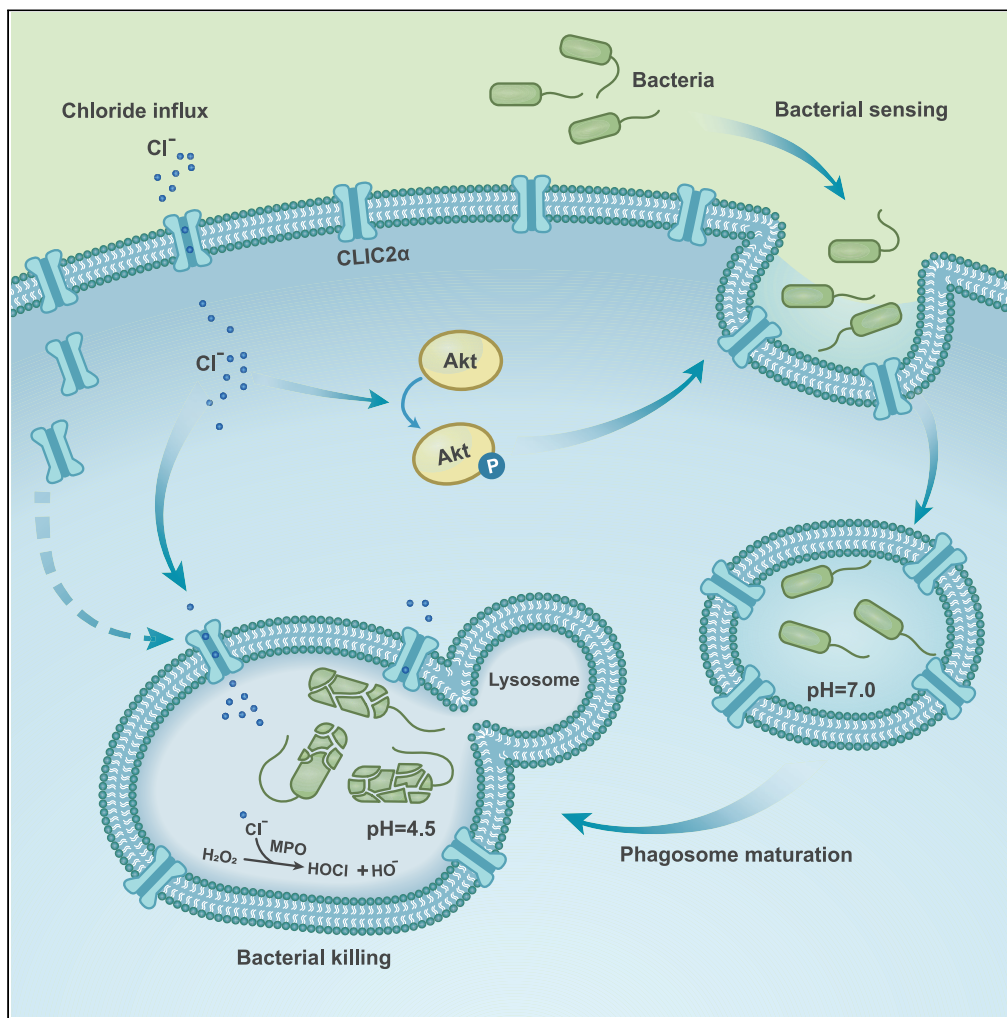**Article**

CLIC2α Chloride Channel Orchestrates Immunomodulation of Hemocyte Phagocytosis and Bactericidal Activity in *Crassostrea gigas*

Xiangyu Zhang, Fan Mao, Nai-Kei Wong, ..., Shu Xiao, Yang Zhang, Ziniu Yu

yzhang@scsio.ac.cn (Y.Z.)
carlzyu@scsio.ac.cn (Z.Y.)

HIGHLIGHTS

Influx of chloride ions is switched on during phagocytosis in oyster hemocytes

PI3K/Akt signaling pathway mediates chloride-dependent activation of phagocytosis

Cl^- promotes phagosomal acidification and HOCl production

CLIC2α is the principal chloride channel encoding gene within oyster genome

iScience

Article

CLIC2α Chloride Channel Orchestrates Immunomodulation of Hemocyte Phagocytosis and Bactericidal Activity in *Crassostrea gigas*

Xiangyu Zhang,[1,2,5] Fan Mao,[1,2] Nai-Kei Wong,[1,3] Yongbo Bao,[4] Yue Lin,[1,2,5] Kunna Liu,[1,2,5] Jun Li,[1,2] Zhiming Xiang,[1,2] Haitao Ma,[1,2] Shu Xiao,[1,2] Yang Zhang,[1,2,6,*] and Ziniu Yu[1,2,*]

SUMMARY

Chloride ion plays critical roles in modulating immunological interactions. Herein, we demonstrated that the anion channel CLIC2α mediates Cl⁻ flux to regulate hemocytes functions in the Pacific oyster (*Crassostrea gigas*). Specifically, during infection by *Vibrio parahemolyticus*, chloride influx was activated following onset of phagocytosis. Phosphorylation of Akt was stimulated by Cl⁻ ions entering host cells, further contributing to signal transduction regulating internalization of bacteria through the PI3K/Akt signaling pathway. Concomitantly, Cl⁻ entered phagosomes, promoted the acidification and maturation of phagosomes, and contributed to production of HOCl to eradicate engulfed bacteria. Finally, genomic screening reveals CLIC2α as a major Cl⁻ channel gene responsible for regulating Cl⁻ influx in oysters. Knockdown of CLIC2α predictably impeded phagosome acidification and restricted bacterial killing in oysters. In conclusion, our work has established CLIC2α as a prominent regulator of Cl⁻ influx and thus Cl⁻ function in *C. gigas* in bacterial infection contexts.

INTRODUCTION

As a principal inorganic anion in the intra- and extracellular environments, chloride (Cl⁻) is involved in an extraordinary range of physiological functions including body fluid retention/excretion, osmotic maintenance, cell volume regulation, and pH balance (Bohn and de Morais, 2017; Rodan, 2019; Wang, 2016). Accumulating evidence has implicated transmembrane Cl⁻ fluxes in antimicrobial processes within immune effectors such as phagocytes, although the underlying mechanisms are not fully understood (Wang, 2016). In mammalian macrophages, phagocytosis is of fundamental importance to innate defenses against invading microbes (Hartenstein and Martinez, 2019). Notably, acidification of phagosomes governs their maturation and eventual antimicrobial capacity (Bouvier et al., 1994), in which Cl⁻ flux is critical to phagosomal pH control and bacterial infection outcomes (Di et al., 2006). Meanwhile, activation of endolysosomal proteases temporally matches the maturation of phagosomes to ensure efficient destruction of engulfed bacteria (Pillay et al., 2002). Some immune-related enzymes, such as cathepsins, show a dependency on Cl⁻ flux for activity via binding to Cl⁻ ion (Cigic and Pain, 1999). In addition, Cl⁻ directly participates in the production of chlorine-containing oxidants for microbial killing in host immunity. Specifically, in neutrophils, myeloperoxidase (MPO), which is enriched in phagosomes, catalytically converts hydrogen peroxide (H_2O_2) and Cl⁻ into the highly potent hypochlorous acid (HOCl), which oxidatively decimates microbes via protein chlorination (Busetto et al., 2007; Rosen et al., 2002, 2009).

Owing to its intrinsic properties of a negatively charged ion, Cl⁻ cannot autonomously permeate cellular membranes; its compartmental distribution instead has to depend on passive transport through specific channels or transporters (Stauber et al., 2012). Since the discovery of the first intracellular Cl⁻ channel protein (p64, later renamed as CLIC5B) in bovines, more members of CLIC proteins were subsequently identified in all phyla, wherein six CLIC genes were found in humans (Landry et al., 1989; Redhead et al., 1992). The CLIC family located in various organelles of the cell is involved in physiological functions and pathological conditions in various human diseases, such as tumor onset and progression, Alzheimer's disease, and cardiac dysfunction (Flores-Tellez et al., 2015; Hernandez-Fernaud et al., 2017; Novarino et al., 2004; Peretti et al., 2015; Takano et al., 2012).

[1]CAS Key Laboratory of Tropical Marine Bio-resources and Ecology, Guangdong Provincial Key Laboratory of Applied Marine Biology, Innovation Academy of South China Sea Ecology and Environmental Engineering (ISEE), South China Sea Institute of Oceanology, Chinese Academy of Science, Guangzhou 510301, P. R. China

[2]Southern Marine Science and Engineering Guangdong Laboratory (Guangzhou), Guangzhou 510301, P. R. China

[3]National Clinical Research Center for Infectious Diseases, Shenzhen Third People's Hospital, The Second Hospital Affiliated to Southern University of Science and Technology, Shenzhen 518112, P. R. China

[4]Zhejiang Key Laboratory of Aquatic Germplasm Resources, College of Biological and Environmental Sciences, Zhejiang Wanli University, Ningbo 315100, P. R. China

[5]University of Chinese Academy of Sciences, Beijing 100049, P. R. China

[6]Lead Contact

*Correspondence:
yzhang@scsio.ac.cn (Y.Z.),
carlzyu@scsio.ac.cn (Z.Y.)

https://doi.org/10.1016/j.isci.2020.101328

Not surprisingly, vertebrate CLICs seem to fulfill indispensable functions as ion channels in helping cells maintain osmotic balance at vesicles and cytoplasm and coordinate interactions between membranes and cytoskeleton (Littler et al., 2010). For example, when low vesicular pH is required, CLICs serve to regulate the actions of proton pumps. CLICs are themselves necessary for the formation and maintenance of intracellular membrane-enclosed vesicles. Elsewhere, substantial evidence based on loss of function of CLIC supports the central importance of these chloride channels in phagocytic defenses. In mice, CLIC1$^{-/-}$ macrophages failed to acidify phagosomes, consequently impairing the cells' capacities for phagosomal proteolysis and reactive oxygen species (ROS) production (Jiang et al., 2012). Likewise, both mice polymorphonuclear leukocytes (PMNs) and human PMNs displayed compromised phagocytic abilities, following CLCN3 knockout (Moreland et al., 2006). In microglial cells, chloride channel blockers suppress formation of engulfment pseudopodia (Harl et al., 2013). Furthermore, CLIC3$^{-/-}$ PMNs also had remarkably reduced NADPH oxidase activity and restricted transendothelial migration. Other than the CLIC family, it should be noted that another specialized Cl$^-$ channel, cystic fibrosis transmembrane conductance regulator (CFTR), was initially identified as a regulator of salt transport across epithelial membranes (Jovov et al., 1995). In patients with cystic fibrosis, the reduced expression of CFTR impaired phagocytosis ability in macrophages (Jovov et al., 1995; Pong et al., 2014). In CFTR-null mutants, macrophages failed to lower phagosomal pH or exhibit adequate bactericidal activity. However, loss of function of CFTR did not seem to impact phagocytic abilities or ROS generation in macrophages (Aiken et al., 2012; Deriy et al., 2009; Di et al., 2006), raising the possibility that different chloride channels may have intrinsically distinct molecular mechanisms for governing aspects of phagocytic defenses. This assumption also applies to the CLC-3 gene, which is expressed in neutrophils as plasma membrane chloride channels, with a clear role in supplying neutralizing anion currents for V-type H$^+$-ATPases that acidify compartments of endosomal/lysosomal pathways (Scheel et al., 2005). In macrophages, CLIC3 was also found essential for CRIg-mediated *Listeria monocytogenes* (LM) killing by directly interacting with the cytoplasmic domain of CRIg (Kim et al., 2013). Indeed, macrophage-specific rescue and knockdown confirmed that CLIC-deficient macrophages failed to clear bacteria (Monahan and Silverman, 2017).

Chloride flux can govern specific signaling pathways to regulate its physiological functions. For example, activation of the ClC-3 chloride channel, responsible for inducing inhibition of the PI3K/Akt/mTOR signaling pathways, has also been proven to determine apoptosis in human nasopharyngeal carcinoma cell lines (CNE-1, CNE-2Z) (Liu et al., 2013). Over-expression of calcium-activated chloride channel A4 (CLCA4) could inhibit cell migration and invasion by suppressing epithelial-mesenchymal transition (EMT) via the PI3K/ATK signaling pathway (Chen et al., 2019). In addition, CLIC1 regulates migration and invasion in gastric cancer by triggering signaling of the ROS-mediated p38 MAPK pathway (Zhao et al., 2015). CLIC1 regulates colon cancer cell migration and invasion through ROS/ERK pathway (Wang et al., 2014). Thus, chloride flux may utilize distinct signaling pathways to execute specific functions in cellular context-dependent manners.

Beyond mammals, the biological roles of Cl$^-$ in other species such as plants and nematodes have been sparingly studied (Chakraborty et al., 2017; Jentsch, 2008; Nguyen et al., 2016). For instance, in *Arabidopsis*, AtClC-e is localized to thylakoid membranes in the chloroplast (Marmagne et al., 2007), where its absence impairs the proton-motive force. Branicky et al. found that the CeClC-3 channel modulates the electrical activity of HSN neurons that control egg laying in *C. elegans* (Branicky et al., 2014). Overall, current knowledge on Cl$^-$ function is mainly limited to mammals and tends to be more fragmentary concerning invertebrates. Despite substantial mammalian evidence that chloride channels are indispensable for robust phagosomal acidification and bactericidal activity (Jentsch, 2008; Moreland et al., 2006), how and to what extent chloride influx and chloride channels contribute to immune defenses in invertebrates is still under-examined. As a marine invertebrate with significant roles in ecological habitats, *Crassostrea gigas* has developed a versatile and intricate innate immune system capable of efficiently recognizing and removing invading pathogens (Wootton et al., 2003). From an evolutionary perspective, hemocytes in oyster are functional analogs of macrophages and neutrophils and are thus assumed to execute at least a subset of immune functions found in their human counterparts (Beaven and Paynter, 1999). Owing to a marine environment with high chloride, many physiological activities including host immune defense in oysters seem to be more dependent and susceptible to chloride than in terrestrial animals. In the present study, we set out to clarify the following cogent issues: (1) potential importance of chloride influx during phagocytosis of oyster hemocytes; (2) regulatory mechanisms that govern immune modulation by Cl$^-$ influx; and (3) the cardinal chloride channel encoding gene that is responsible for Cl$^-$ fluxes control in oyster hemocytes.
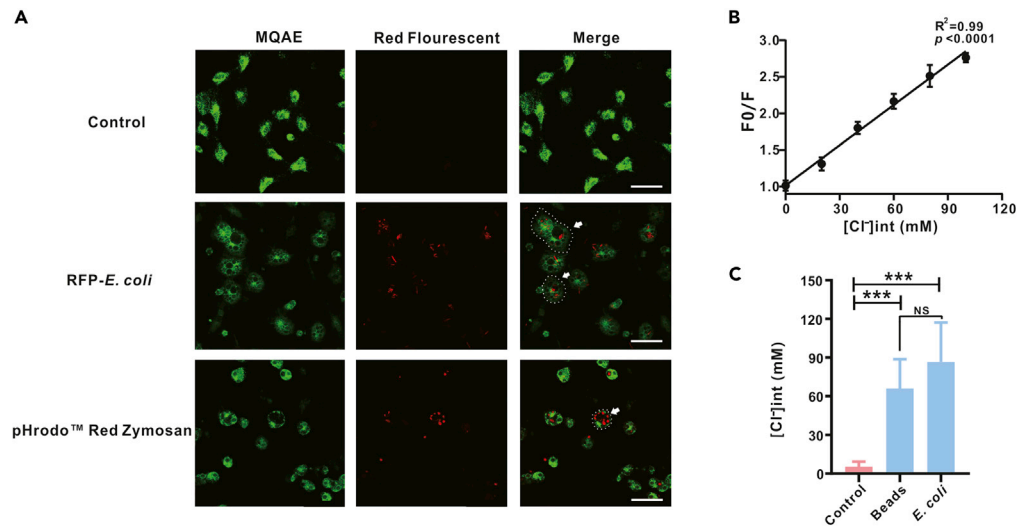
Figure 1. Chloride Influx Is Activated during Phagocytosis

(A) Fluorescence of phagocytosed cells was significantly reduced. Oyster hemocytes loaded with MQAE (green) were challenged with pHrodo Red zymosan and fluorescent bacteria for 30 min at 27°C. MQAE is a fluorescent indicator that is quenched on encountering chloride. Cells were then imaged with a Leica SP8 inverted confocal microscope. White arrows indicate cells with significantly reduced fluorescence. Outline of cells pinpointed by an arrow is delineated by a dashed white line. MQAE signals of the experimental group were measured only in phagocytic cells. Scale bar: 10 μm.

(B) Stern-Volmer calibration curve in HEPES-buffered standard solutions for MQAE (a Cl^--sensitive fluorescent dye) loaded into oyster hemocytes. Data are presented as mean $\pm$ SD.

(C) $[Cl^-]_i$ in oyster hemocytes after phagocytosing beads and *E. coli* rose significantly. Fluorescence intensities of MQAE in oyster hemocytes at rest and hemocytes phagocytosing beads and *E. coli* were extracted to estimate $[Cl^-]_i$. Data were analyzed by using Image-Pro Plus 6.0. Data were analyzed by unpaired t test and presented as mean $\pm$ SD, ***p < 0.001, NS: no significant difference, n = 3 groups, each group contains 10–15 cells.

RESULTS

Chloride Influx Is Activated during Phagocytosis

To explore the possible immunodulatory roles of Cl^- influx in oyster hemocytes, we first examined whether Cl^- influx is activated during phagocytosis. Levels of intracellular Cl^- concentration ($[Cl^-]_i$) were measured by using the Cl-specific fluorescent probe MQAE. MQAE's fluorescence intensity decreases proportionally with increasing chloride ion concentration. Cell viability assay showed that hemocytes cultured *in vitro* keep a high cell viability under a broad range of temperature (Figure S1). Intriguingly, we observed a significant decrease in fluorescence intensity of MQAE (green Cl^- sensor) in phagocytes (red-fluorescence positive cells), upon hemocyte engulfment of either pHrodo Red zymosan or *E. coli* (Figure 1A), indicating an elevation of intracellular Cl^- concentration $[Cl^-]_i$ during phagocytosis. To calibrate $[Cl^-]_i$, a standard curve for MQAE fluorescence intensity versus $[Cl^-]_i$ was constructed by using a series of buffers prepared across a Cl^- concentration gradient (Koncz and Daugirdas, 1994) (Figure 1B). On the basis of no significant difference in the phagocytosis rate of pHrodo Red zymosan and *E. coli* (Figures S2A and S2B), calibrated by standard curve, $[Cl^-]_i$ was markedly increased from a baseline of 4.85 $\pm$ 4.49 to 65.74 $\pm$ 22.90 mM when hemocytes phagocytized zymosan-coated latex beads, and to 86.52 $\pm$ 30.71 mM in the case of *E. coli* (Figure 1C). However, no significant difference in magnitude of Cl^- influx was observed during phagocytosis whether for pHrodo Red zymosan or *E. coli*, suggesting that activation of Cl^- influx is a cellular event tightly coupled to phagocytosis initiation, regardless of the nature of phagocytosed substrates.

Chloride Channel Inhibitor Blocks Phagocytosis in Hemocytes

To determine the function of Cl^- influx on phagocytic capacities of hemocytes, IAA-94, a potent indanyloxyacetic acid blocker of CLIC family channels, was employed in subsequent assays. In terms of intracellular Cl^- availability in oyster hemocytes, treatment of IAA-94 (100 μM) efficiently blocked infection-induced Cl^- influx activation (Figure S3), where the average steady-state $[Cl^-]_i$ of phagocytized hemocytes at 30 min post infection was dramatically reduced from 86.52 $\pm$ 30.71 to 36.33 $\pm$ 7.5mM, when compared
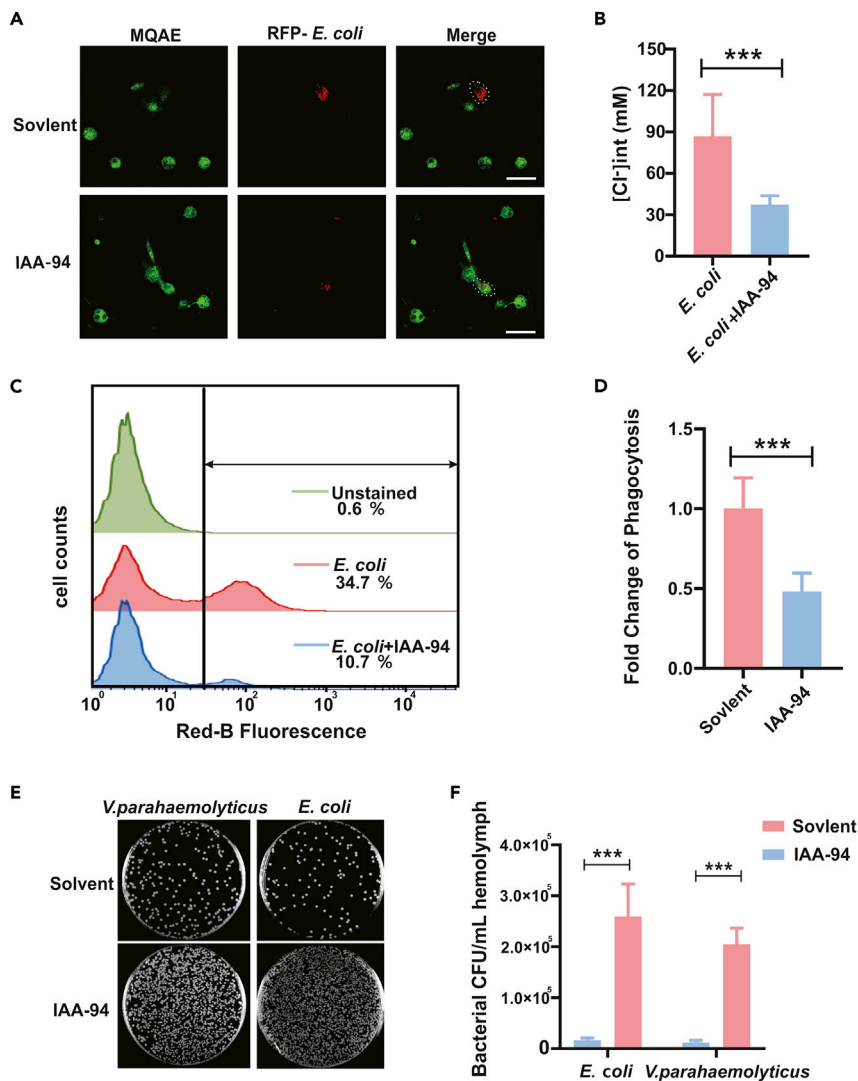
Figure 2. Chloride Channel Inhibitor Blocks Phagocytic Ability in Hemocytes

(A) Fluorescence of IAA-94 treated phagocytes was enhanced. Oyster hemocytes engulfing fluorescent bacteria were loaded with MQAE (green). An intervention group was co-treated with IAA-94. Cells were imaged with a Leica SP8 inverted confocal microscope. Scale bar: 10 μm. IAA-94 is a potent indanyloxyacetic acid blocker of epithelial chloride channels. Outline of the cells is delineated by a dashed white line. MQAE signals were measured in phagocytic cells engulfing *E. coli*.

(B) $[Cl^-]_i$ of IAA-94-treated phagocytes decreased. MQAE fluorescence intensities in oyster hemocytes treated with IAA-94 were extracted to estimate $[Cl^-]_i$. Data were analyzed by using Image-Pro Plus 6.0. Data were analyzed by unpaired t test and presented as mean $\pm$ SD, ***$p < 0.001$, $n = 3$.

(C) IAA-94 inhibited phagocytosis of *E. coli* by hemocytes. Under the premise that the number of cells in each group was approximately the same, flow cytometry analysis was conducted to gauge the extent of hemocytic phagocytosis. Red color represents the solvent-treated control and blue color represents the group treated with IAA-94.

(D) Data analysis was performed by using GraphPad Prism 7 software. Data were analyzed by unpaired t test and presented as mean $\pm$ SD, ***$p < 0.001$, $n = 3$.

(E) IAA-94 inhibited bactericidal ability of hemocytes. Display of differences in bactericidal ability between the control group and the IAA-94-treated group.

(F) Assay on bactericidal ability was analyzed by using GraphPad Prism 7. Data were analyzed by unpaired t test and presented as mean $\pm$ SD, ***$p < 0.001$, $n = 3$.

with IAA-94 treatment group (Figures 2A and 2B). Meanwhile, the capacity of hemocyte to engulf bacteria was sharply reduced in the presence IAA-94, when compared with the basal control (treatment with solvent) (Figure S4). In agreement with this, the inhibitory effects of IAA-94 on hemocyte phagocytosis

were confirmed in a quantitative manner by flow cytometry analysis (Figure 2C). The results suggest that IAA-94-treated group had an engulfment capacity approximately 50% less than that of the control group (Figure 2D). Understandably, the sequential processes of containment and killing of microbial pathogens are inseparable components of phagocyte-mediated defenses. Indeed, in bacterial killing assays, bactericidal capacity of hemocytes was greatly compromised after blockage of Cl^- influx. In contrast to the basal control, 30 min post infection, bacterial survival in IAA-94-treated hemocytes starkly increased (Figures 2E and 2F). Therefore, these observations strongly implicate that Cl^- influx is critical for phagocytic defense in oyster hemocytes through promoting capacity of engulfment and microbicidal activity.

Chloride-Dependent Engulfment Is Promoted by PI3K/Akt Signaling Pathway

As a classical signaling pathway for regulating phagocytosis, the PI3K/Akt signaling pathway has been shown to be activated by chloride influx, leading to the hypothesis that PI3K/Akt signaling pathway may be a key regulator that controls or promotes Cl^--dependent phagocytosis in oyster hemocytes. As anticipated, phagocytic capacity of oyster hemocytes was significantly boosted (1.53-fold) upon treatment of a PI3K activator (740Y-P, 30 μM) compared with the control. Contrarily, phagocytic capacity was suppressed to 51% when hemocytes were co-treated with a PI3K inhibitor (LY294002, 1 μM), thus implicating the PI3K signaling pathway as an essential regulator for phagocytosis in oyster hemocytes (Figure 3A). More importantly, 740Y-P evidently rescued phagocytic impairments induced by IAA-94 in hemocytes, which raises the possibility of a functional interplay between PI3K/Akt signaling pathway and Cl^- influx mediating phagocytosis (Figure 3B). Furthermore, western blot analysis shows that the Akt phosphorylation increased substantially by 1.60- and 1.10-fold in infected and 740Y-P-treated oyster hemocytes, respectively, with respect to the control group. IAA-94 dampened Akt phosphorylation under both bacterial infection and untreated conditions, compared with the control group (Figures 3C and 3D). Taken together, these results support the notion that Cl^--dependent phagocytosis is likely promoted by the PI3K/Akt signaling pathway.

Chloride Ion Flux Modulates Phagosomal Acidification and HOCl Production without Affecting Phagosomal-Lysosomal Fusion

Since coordinated Cl^- ion flux is essential for pH regulation toward phagosomal acidification and catalytic production of HOCl, we examined whether these immunomodulatory roles of Cl^- are mechanistically conserved in the Pacific oyster. pHrodo Red dye (a fluorescent pH sensor) conjugated particles were used to determine any fluctuations in phagosomal acidification, whose signals show a negative correlation between its fluorescence intensity with pH (Figure S5). Following treatment of IAA-94 (100 μM), the intensity of phagosome-related fluorescence visibly declined at 15 and 30 min post phagocytosis (Figures 4A and 4B), which corroborates the assumption of Cl^- ion flux as an important modulator for phagosomal acidification in oyster hemocytes. To test whether additional factors can impede Cl^--dependent bacterial clearance in hemocytes, the hemocytic capacity for HOCl biosynthesis was assessed by an *in vivo* HOCl assay, with a standard curve constructed to calibrate the amounts of TNB versus optical density (HOCl levels) being determined (Figure S6). *V. parahaemolyticus* infection elicited 1.33-fold more HOCl, in comparison with the control group (Figure 4C), but this was abolished in the presence of IAA-94, implicating Cl^- ion flux as a significant regulator at work in infection-induced HOCl production. In addition, we also attempted to ask whether Cl^- ion flux impacts phagosomal-lysosomal fusion, as it is a critical step toward phagosomal maturation and bactericidal activity. However, our results show no appreciable differences between IAA-94-treated group and untreated group up to 60 min post phagocytosis (Figure 4D).

CLIC2α Is a Primary Chloride Ion Channel within Oyster Genome

To illuminate the genetic basis of Cl^- ion flux control in this ancient marine invertebrate, we set out to examine the gene families encoding the Cl^- channel in oyster and perform homologs search-based alignment on a genomic scale. Intriguingly, only two members of the CLIC family were identified in the Pacific oyster genome, whereas all CTFR homologs are absent (Figure 5A). A phylogenetic tree was then generated based on CLIC superfamily protein sequences from different species including *Homo sapiens*, *Mizuhopecten yessoensis*, *Xenopus tropicalis*, *Danio rerio*, *Drosophila melanogaster*, and *Crassostrea gigas*, which reveals that the CLIC family has highly diversified during evolution and considerably expanded in vertebrates, whereas the homologs of CTFR only prevail in vertebrate lineages (Figures 5B and S7). Based on the results of the evolutionary tree, we observed that CLIC2 is the only highly conserved Cl^- channel retained among ancient species such as *Protostomia* and *Deuterostomia*. Specifically, the ortholog of CLIC2 is duplicated in the genome of *C. gigas*, namely, CLIC2α and CLIC2β (Figure 5C). Tissue distribution
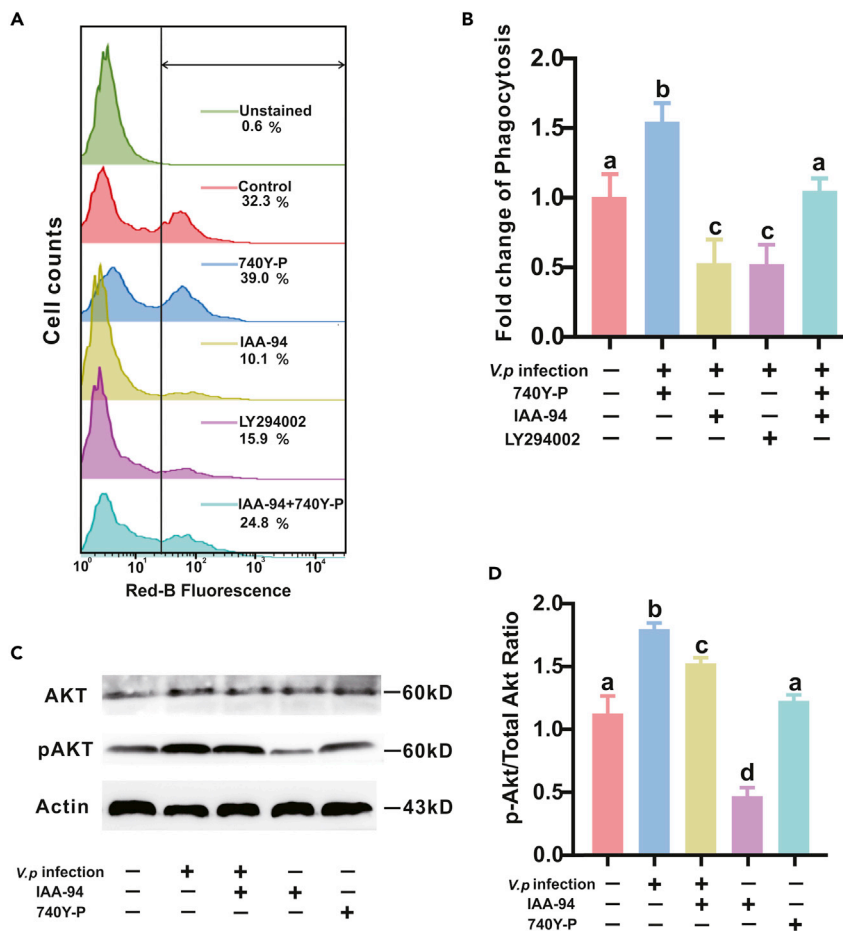
Figure 3. Chloride-Dependent Phagocytosis Is Regulated by PI3K/Akt Signaling Pathway

(A) PI3K/Akt signaling pathway is involved in chloride-mediated phagocytosis. Flow cytometry analysis was used to detect hemocytic phagocytosis following bacterial infection in the presence or absence of pharmacological inhibitors as indicated. 740Y-P is a potent cell-permeable PI3K signaling activator. LY294002 is a broad-spectrum inhibitor of PI3K signaling.

(B) Phagocytosis data analysis was performed by using GraphPad Prism 7 software. Data were analyzed by one-way ANOVA followed by Tukey's post hoc test, where $p < 0.05$ was considered to be statistically significant, as denoted by different letters. Data are presented as mean $\pm$ SD, $n = 3$.

(C) Western blot analysis on the effects of pharmacological intervention on bacterial infection: IAA-94 versus 740 Y-P with respect to the expression of proteins related to PI3K/Akt/mTOR signaling pathway. Levels of p-Akt/Akt was evaluated by western blot analysis. β-Actin served as a loading control.

(D) p-Akt/Akt expression was measured densitometrically by using ImageJ. The data are normalized to β-Actin. Data analysis was performed by using GraphPad Prism 7 software. Data were analyzed by one-way ANOVA followed by Tukey's post hoc test, where $p < 0.05$ was considered to be statistically significant, as denoted by different letters. Data are presented as mean $\pm$ SD, $n = 3$.

showed that CLIC2α is predominantly expressed in hemocytes (Figure 5D), which suggests a key role of CLIC2α in regulating Cl^- transportation during hemocytes phagocytosis.

To further clarify the roles of hemocyte CLIC2α in immunological contexts, we attempted to determine the subcellular localization of CLIC2α by immunofluorescence. The antibody was verified by western blotting to ensure that the antibody specifically binds to the antigen stated (Figure 5E). Compared with non-immune IgG group, immunofluorescence showed that CLIC2α staining patterns were punctate or patchy within resting hemocytes, with evidently dense foci around the cell membrane in the resting hemocytes (Figures 5F and S8). Moreover, we also examined the subcellular localization of CLIC2α upon phagocytosis. The results show an evident overlay between CLIC2α positive signaling and FITC-beads (Figure 5F), implying phagosomal localization of CLIC2α in oyster hemocytes.
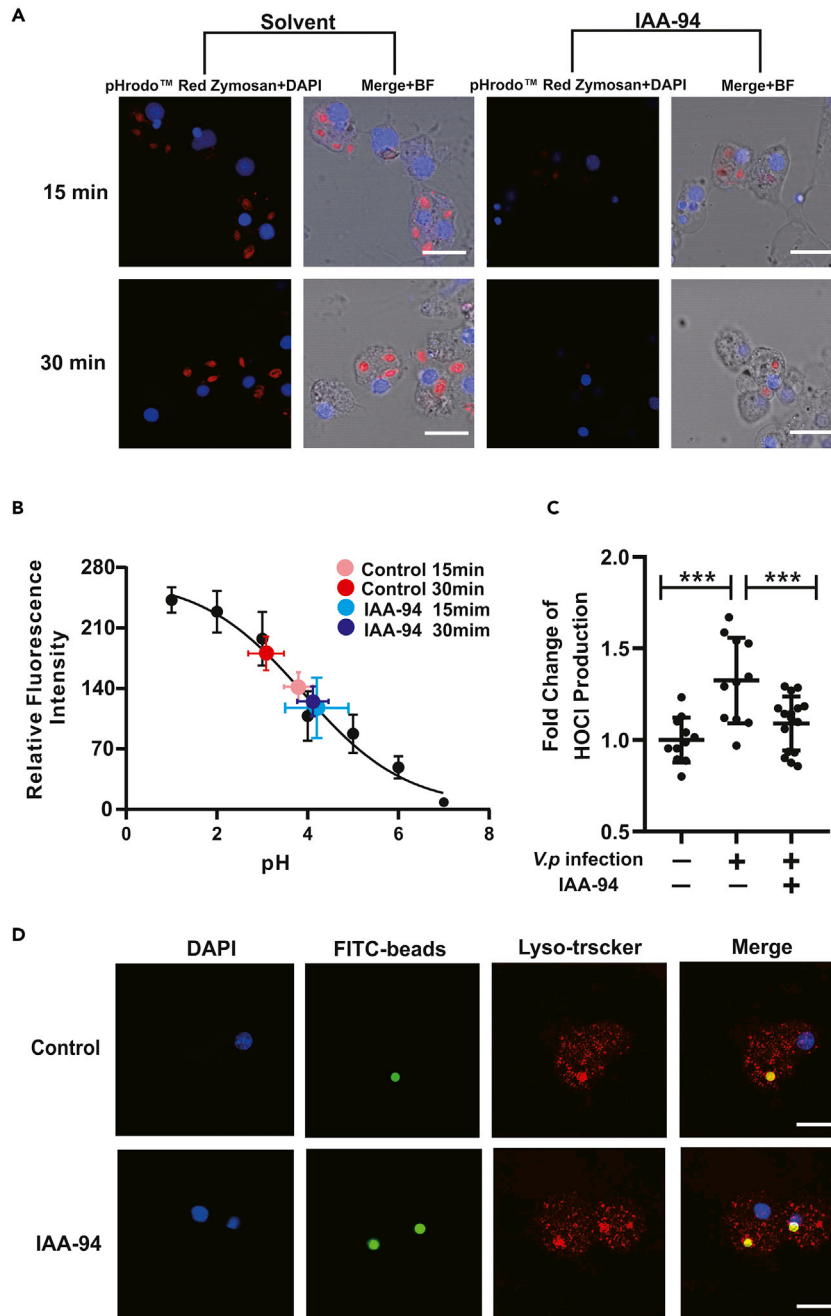
Figure 4. Chloride Flux Affects Phagosomal Acidification and HOCl Production but Not Phagosomal-Lysosomal Fusion

(A) Acidification defects in phagosomes following particles ingestion in oyster hemocytes treated with IAA-94. Cells that had ingested pHrodo Red zymosan were observed by confocal microscopy. Scale bar: 5 μm.

(B) Intraphagosome pH values are interpolated on a standard curve for pHrodo Red zymosan fluorescence versus pH determined *in vitro* by using a series of buffers. Fluorescence emission was calibrated and a fluorescence index was obtained from the samples ($n = 3$ groups, each group contains 10–15 cells). Bars represent as mean $\pm$ SD.

(C) Following *in vivo* infection of oysters ($n = 6$ per group) with *V. parahaemolyticus*, in the presence or absence of IAA-94, HOCl production was assessed. Data analysis was performed by using GraphPad Prism 7 software. Data were analyzed by unpaired t test and presented as mean $\pm$ SD, ***$p < 0.01$.

(D) Representative confocal images of hemocytes during observations of phagosomal-lysosomal fusion 60 min from onset of phagocytosis. LysoTracker red is a red fluorescent probe for lysosomes that can be used for lysosome-specific fluorescent staining of living cells. Scale bar: 3 μm.
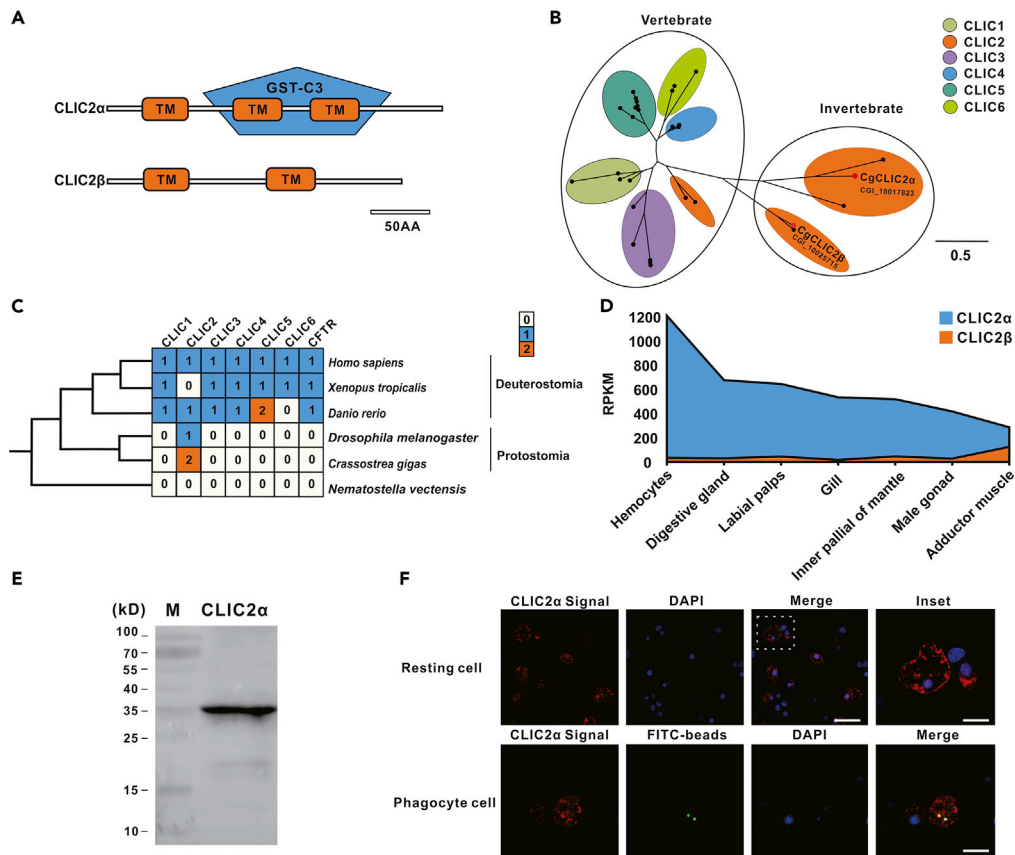
Figure 5. CLIC2α Is One of the Main Cl⁻ Channels in Oyster Genome and Subcellular Localization of CLIC2α in Oyster Hemocytes

(A) Schematic representation of a comparison between transmembrane structures of intracellular Cl⁻ channel proteins in *C. gigas*.

(B) CLIC superfamily protein sequences from different species including *Homo sapiens, Mizuhopecten yessoensis, Xenopus tropicalis, Danio rerio, Drosophila melanogaster*, and *C. gigas*.

(C) Distribution patterns of six CLIC and CFTR genes. White, ortholog absent; blue, single-copy ortholog present; orange, double-copy ortholog present.

(D) Analysis on expression levels of two intracellular Cl⁻ channel proteins in *C. gigas*. The *y* axis shows expression levels, and the *x* axis shows tissue sources.

(E) Figure for western blot analysis of CLIC2α antibodies.

(F) Immunofluorescence confocal micrographs show the spatial distribution of CLIC2α (red) as detected by a CLIC2α-specific primary antibody within oyster hemocytes. Nuclei (blue) were counterstained with DAPI. Scale bar: 5 μm. The insets show higher magnification. Scale bar of insets: 3 μm. Scale bar of phagocyte group: 4 μm.

Immunological Relevance of CLIC2α in Oyster Hemocytes

To verify the function of CLIC2α as a Cl⁻ channel in oyster hemocytes, RNAi experiments were performed to knock down expression of CLIC2α. Results from quantitative PCR suggest that relative expression of CLIC2α was reduced by about 60% with respect to the dsGFP control group (Figure 6A), which is consistent with the knockdown efficiency at the protein level as verified by western blot (Figures 6B and 6C). As a test for validating Cl⁻ flux, fluorescence intensity of MQAE in the dsCLIC2α group was shown to be much enhanced compared with that of the dsGFP group in hemocytes under condition of *in vivo* infection by live *V. parahaemolyticus* (Figures 6D and 6E). Collectively, these observations confirm that CLIC2α is a conserved and functionally relevant Cl⁻ channel in oyster hemocytes.

As CLIC2α is known to serve as a Cl⁻ channel that controls the flow of Cl⁻ ion into the cytosol, it is reasonable to conclude that CLIC2α resides on the hemocytic cell membrane to exercise this function. Given the abundance of CLIC2α in hemocytes (Figure 5D), we reasoned that CLIC2α protein is responsible for Cl⁻-
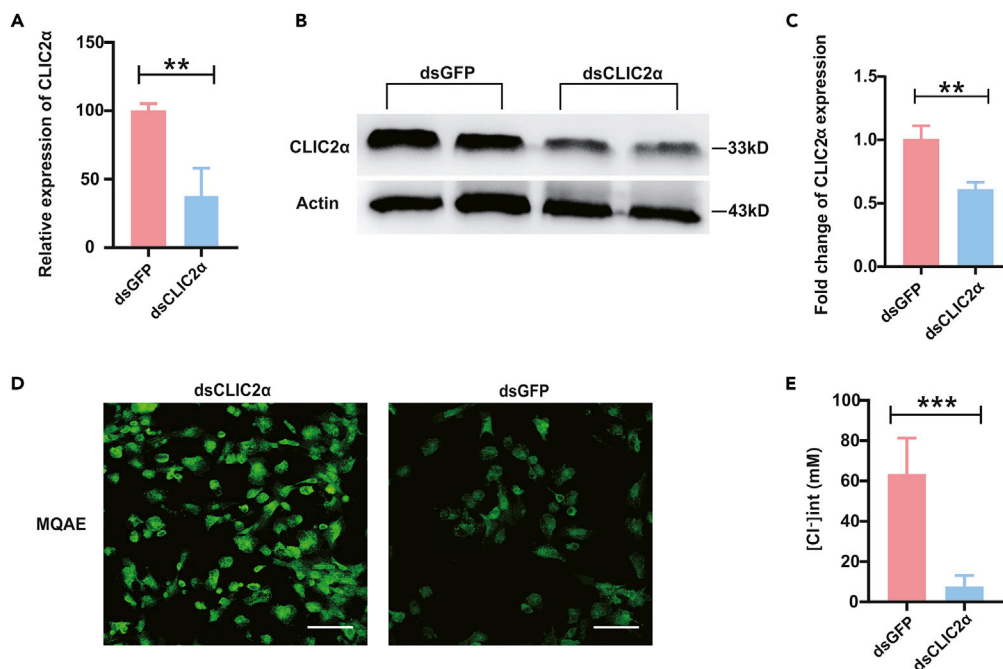
Figure 6. CLIC2α Is Responsible for Cl⁻-Mediated Innate Immunity in Oysters

(A) Relative expression of CLIC2α is shown after RNAi in oyster hemocytes. Red color represents the dsGFP control group and blue color represents the dsCLIC2α group. mRNA levels were quantified by real-time PCR with GAPDH as a reference gene. Data were analyzed by unpaired t test and presented as mean ± SD, **p < 0.01, $n = 3$.

(B) Western blot analysis on the effects of RNAi. Levels of CLIC2α was evaluated by immunoblotting. β-Actin served as a loading control.

(C) CLIC2α expression was measured densitometrically by using ImageJ. Data analysis was performed by using GraphPad Prism 7 software. Data were analyzed by unpaired t test and presented as mean ± SD, **p < 0.01, $n = 3$.
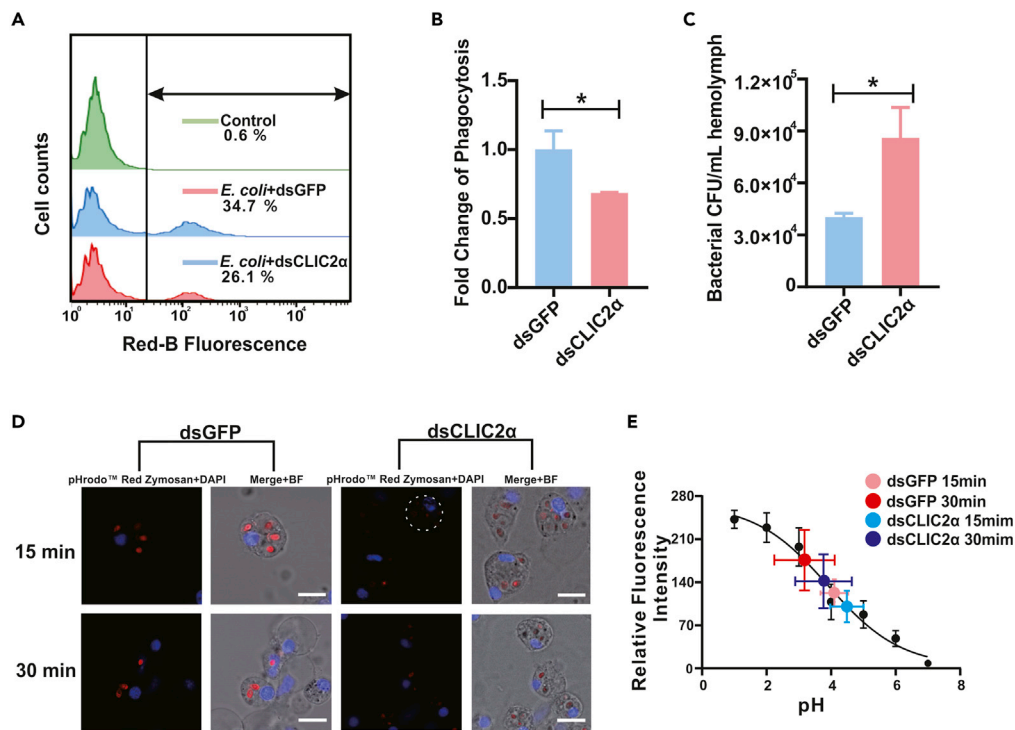
(D) Confocal micrographs show the fluorescence intensities of the dsCLIC2α and dsGFP groups of *Vibrio*-exposed hemocytes. Scale bar: 15 μm.

(E) Data analysis was performed by using GraphPad Prism 7 software. Fluorescence intensities were normalized by cell number and volume of hemocytes. Data were analyzed by unpaired t test and presented as mean ± SD, ***p < 0.001, $n = 3$.

mediated phagocytic defenses during *in vivo* infection by live *V. parahaemolyticus*. Quantitative analysis by flow cytometry (Figure 7A) shows that CLIC2α knockdown resulted in a reduction of 32% in phagocytic capacity of hemocytes compared with the control group (Figure 7B). Bacterial survival counts of infecting *V. parahaemolyticus* rose from 3.98×10^4 to 8.55×10^4 CFU following RNAi of CLIC2α (Figure 7C). Furthermore, knockdown of CLIC2α in hemocytes clearly compromised their ability to acidify phagosomes (Figures 7D and 7E), which likely has adverse consequences for bacterial clearance. Overall, these results implicate RNAi of CLIC2α with impaired hemocytic phenotypes in phagocytosis, phagosomal acidification, and microbial killing, thus supporting an essential role of CLIC2α in Cl⁻-mediated innate immunity in oysters.

DISCUSSION

Chloride ion is a ubiquitous yet indispensable constituent in phagocyte biology. It is responsible for mediating numerous physiological functions including maintenance of membrane potential, regulation of phagosomal pH, promotion of phagosomal enzymatic activities, and production of Cl⁻-containing oxidants as antimicrobial agents (Wang, 2016). Chloride ion channels (CLICs) have been intimately linked to inflammatory diseases, inspiring enduring interest in their immune roles (Gururaja Rao et al., 2020). Despite substantial advances in vertebrates, mechanistic understanding on the immune function of Cl⁻ in invertebrates remains scant. Here, we have revealed for the first time that coordinated phagocytic events associated with Cl⁻ flux occur after infection and that an under-examined Cl⁻ channel, CLIC2α, plays vital roles in promoting hemocyte phagocytosis and bactericidal activity of *C. gigas*, a representative species in lower marine invertebrates.

Figure 7. Immunological Relevance of CLIC2α in Oyster Hemocytes

(A) Relative to the control group, ability of the dsCLIC2α group to swallow *E. coli* declined. Flow cytometry analysis was conducted to detect hemocytes phagocytosis of fluorescently labeled bacteria. Red color represents the dsGFP control group and blue color represents the dsCLIC2α group.

(B) Data analysis for hemocytes phagocytosis was performed by using GraphPad Prism 7 software. Data were analyzed by unpaired t test and presented as mean $\pm$ SD, *p < 0.0, n = 3.

(C) Relative to the control group, the bactericidal ability of the dsCLIC2α group decreased. Assay on bactericidal ability of the dsCLIC2α group and the dsGFP control group was analyzed by using GraphPad Prism 7 software. Data were analyzed by unpaired t test and presented as mean $\pm$ SD, *p < 0.05, n = 3.

(D) Acidification defects in phagosomes following particle engulfment in oyster hemocytes silenced by dsCLIC2α, in comparison with dsGFP group. Cells that had ingested pHrodo Red zymosan were observed by confocal microscopy. Scale bar: 5 μm.

(E) Fluorescence emission was calibrated and a fluorescence index was obtained from the samples (n = 3 groups, each group contains 10–15 cells). Bars represent mean $\pm$ SD.

Functional diversity abounds in the regulation and direction of Cl$^-$ flow/flux across different cell types. For instance, intracellular Cl$^-$ concentration was markedly elevated in human airway epithelial BEAS-2B cells upon challenge with LPS (lipopolysaccharide) from *P. aeruginosa* (Zhang et al., 2018). In a similar case, [Cl$^-$]$_i$ of resting oyster hemocytes is kept at a low level but surges upon infections. In contrast, Cl$^-$ efflux ensued when human neutrophils were exposed to *Candida albicans* opsonized with various soluble factors (Busetto et al., 2007). The reason for the different flow directions of Cl$^-$ is uncertain and may concern how different cells interact with exogenous danger signals. Regardless, productive acidification of phagosomes is invariably a mandatory requirement for proper phagocytic functions. Phagosomal pH is primarily controlled by activity of H$^+$-pumping vacuolar-type ATPases (V-ATPase) and importation of anions (Kissing et al., 2018). Proton pumping, which depresses luminal pH, generates an electrochemical potential difference across membranes (positive charge on the luminal side). If left unchecked, this driving force would begin to decelerate and eventually inhibit further acidification (Grabe et al., 2000; Kettner et al., 2003). To prevent premature inhibition, the generated voltage is offset by import of anions (Cl$^-$) and/or export of cations (Kissing et al., 2018). As a result, inappropriate or insufficient Cl$^-$ flux can be an important cause of impaired phagosomal acidification. With the efflux of Cl$^-$ ions, neutrophil phagosomes initially alkalinize and slowly acidify to a moderate level (El Chemaly et al., 2014; Jankowski et al., 2002). Additionally, ClC3 chloride channel is reportedly expressed in neutrophils and their phagosomes, modulating phagosomal pH (Scheel et al., 2005). Deletion of CFTR in murine alveolar macrophages caused defective phagosomal

acidification and bactericidal activity (Deriy et al., 2009; Di et al., 2006). Consistent with these previous findings, we have demonstrated blocking of Cl⁻ flux disrupts phagosome acidification and thus its phagocytic function in oyster hemocytes.

An acidic environment exerts modulatory effects on the structural maturation of hydrolases and denaturation of their protein substrates, which ultimately increases the rates of killing engulfed bacteria (Pillay et al., 2002). For complementing this mode of antibacterial defense, phagocytes also use a combination of oxidative mechanisms, including the production of superoxide ($O_2^{\bullet-}$) and hypochlorous acid (HOCl), to eradicate phagocytosed microorganisms (Kobayashi et al., 2000). Superoxide produced in phagocytes is unstable and has only mild antimicrobial potential. Instead of directly leveraging $O_2^{\bullet-}$, phagocytes convert it to hydrogen peroxide (H_2O_2), a long-lasting oxidant with modest antimicrobial activity at millimolar level (Bonvillain et al., 2011; Lymar and Hurst, 1995). Subsequently, H_2O_2 is turned into the much more potent HOCl via MPO (Bonvillain et al., 2011). Evolutionarily, regulated production of ROS such as HOCl represents a major advance in phagocytic innate immunity (Albrich et al., 1981). In this study, we found that oysters have evolved an efficient machinery to produce these oxidizing biocides. Under conditions of bacterial stimulation, production of HOCl increased, whereas blocking Cl⁻ flux resulted in its inhibition.

Apart from implications in ROS production, Cl⁻ flux seems to mediate hemocytic functions in PI3K/Akt-dependent manners. Previous research findings have shown that PI3K plays an indispensable role in phagosome formation and maturation. During initial phagocytosis, PI3K controls actin depolymerization to drive the formation of a phagocytic cup that surrounds a foreign body and bring it into the phagosome (Olazabal et al., 2002; Tuxworth et al., 2001). Pharmacological inhibition of PI3K could impair the ability of phagocytosis (Araki et al., 1996, 2003; Cox et al., 1999). Moreover, PI3K/Akt/mTOR signaling regulates phagosome maturation by modulating microtubule-based motor activity to modulate events of lysosome trafficking and fusion in leukocytes (Saric et al., 2016). Consistently, our study confirms that PI3K/Akt signaling in the regulation of phagocytosis is conserved from oyster to mammals. More importantly, the PI3K/Akt pathway is crucial to mediating Cl⁻ flux-dependent phagocytosis, which is supported by the evidence that the PI3K activator 740Y-P could rescue blockage of phagocytosis caused by chloride channel inhibitors IAA-94. However, the chloride channel inhibitors IAA-94 had no effects on the fusion of lysosomes and phagosomes as reported in macrophages (Jiang et al., 2012), which seems to contradict with the anticipated roles of PI3K/Akt in phagosome maturation. One possibility is that Cl⁻ flux may activate other signaling pathways or regulatory mechanisms of intracellular feedback to brake on the fusion of lysosomes and phagosomes, which remains to be verified.

In this study, phylogenetic analysis with functional validation showed that CLIC2α is the primary Cl⁻ channel in oyster, and we thoroughly investigated the potential roles of the Cl⁻ channel CLIC2α in innate immunity in oyster hemocytes. CLIC2α was identified as a CLIC family member protein with the highest expression levels in the oyster. CLICs are highly conserved in chordates with six vertebrate paralogs, from CLIC1 to CLIC6. According to the phylogenetic tree, only CLIC2 exists in invertebrates and expands to CLIC2α and CLIC2β. From an evolutionary perspective, CLIC2 appears to be the only one Cl⁻ channel with function conserved from an ancestral progenitor of *Protostomia* and *Deuterostomia*. Subcellular localization of one specific protein is generally associated with its function and also provides clues on regulatory mechanisms. In mammalian macrophages, CLIC1 occurs as spots in the cytoplasm and is translocated to the phagosomal membrane during phagocytosis (Jiang et al., 2012). In contrast, CLIC2α in oysters is mainly localized in the cellular membrane but could be translocated to the phagosomal membrane in manners resembling macrophage CLIC1. Given that composition-wise the phagosomal membrane originates from the plasma membrane, membrane trafficking may be one possible route for CLIC2α translocation. Furthermore, knocking down CLIC2α evidently diminished Cl⁻ flux and disrupted Cl⁻-dependent phagocytic functions in oyster hemocytes, including phagocytosis, phagosomal acidification, and bacterial killing. Beyond the current scope of investigation on phagocytic immunity, it is quite likely that CLIC2α performs other biological functions central to cell physiology in vertebrates and invertebrates alike. Future studies on novel CLIC2α functions and their underlying mechanisms are thus warranted.

Limitations of the Study

In this study, we have explored the subcellular localization and function of CLIC2α mainly in bacterial infection contexts. Further in-depth characterization of the exact roles of CLIC2α in governing the downstream of PI3K/Akt or other intracellular signaling pathways in immune defense and how CLIC2α could be activated would be pertinent.

Resource Availability

Lead Contact

Further information and requests for resources should be directed to and will be fulfilled by the Lead Contact, Yang Zhang (yzhang@scsio.ac.cn).

Materials Availability

All unique/stable reagents generated in this study are available, on reasonable request, from the Lead Contact on a completed Materials Transfer Agreement.

Data and Code Availability

All data supporting the findings of this study are included in the article and its Supplemental Information or are available from the corresponding authors on request.

METHODS

All methods can be found in the accompanying Transparent Methods supplemental file.

SUPPLEMENTAL INFORMATION

Supplemental Information can be found online at https://doi.org/10.1016/j.isci.2020.101328.

AUTHOR CONTRIBUTIONS

Conceptualization: Y.Z. Methodology and Investigation: X.Z., F.M., Y.L., K.L. Resources: Z.X., Y.Z., J.L., H.M., Y.B., S.X. Writing – Original draft: X.Z. All authors read and provided input on the manuscript. Writing – Review and Editing: Y.Z., N.-K.W., X.Z. Supervision and Project Administration: Y.Z., Z.Y. Funding Acquisition: Y.Z., Z.Y.

DECLARATION OF INTERESTS

The authors declare that there no conflicts of interest.

REFERENCES

Aiken, M.L., Painter, R.G., Zhou, Y., and Wang, G. (2012). Chloride transport in functionally active phagosomes isolated from Human neutrophils. Free Radic. Biol. Med. *53*, 2308–2317.

Albrich, J.M., McCarthy, C.A., and Hurst, J.K. (1981). Biological reactivity of hypochlorous acid: implications for microbicidal mechanisms of leukocyte myeloperoxidase. Proc. Natl. Acad. Sci. U S A *78*, 210–214.

Araki, N., Hatae, T., Furukawa, A., and Swanson, J.A. (2003). Phosphoinositide-3-kinase-independent contractile activities associated with Fcgamma-receptor-mediated phagocytosis and macropinocytosis in macrophages. J. Cell Sci. *116*, 247–257.

Araki, N., Johnson, M.T., and Swanson, J.A. (1996). A role for phosphoinositide 3-kinase in the completion of macropinocytosis and phagocytosis by macrophages. J. Cell Biol. *135*, 1249–1260.

Beaven, A.E., and Paynter, K.T. (1999). Acidification of the phagosome in *Crassostrea virginica* hemocytes following engulfment of zymosan. Biol. Bull. *196*, 26–33.

Bohn, A.A., and de Morais, H.A. (2017). A quick reference on chloride. Vet. Clin. North. Am. Small Anim. Pract. *47*, 219–222.

Bonvillain, R.W., Painter, R.G., Ledet, E.M., and Wang, G. (2011). Comparisons of resistance of CF and non-CF pathogens to hydrogen peroxide and hypochlorous acid oxidants in vitro. BMC Microbiol. *11*, 112.

Bouvier, G., Benoliel, A.M., Foa, C., and Bongrand, P. (1994). Relationship between phagosome acidification, phagosome-lysosome fusion, and mechanism of particle ingestion. J. Leukoc. Biol. 55, 729–734.

Branicky, R., Miyazaki, H., Strange, K., and Schafer, W.R. (2014). The voltage-gated anion channels encoded by clh-3 regulate egg laying in C. elegans by modulating motor neuron excitability. J. Neurosci. 34, 764–775.

Busetto, S., Trevisan, E., Decleva, E., Dri, P., and Menegazzi, R. (2007). Chloride movements in human neutrophils during phagocytosis: characterization and relationship to granule release. J. Immunol. 179, 4110–4124.

Chakraborty, K., Leung, K., and Krishnan, Y. (2017). High lumenal chloride in the lysosome is critical for lysosome function. Elife 6, e28862.

Chen, H., Liu, Y., Jiang, C.J., Chen, Y.M., Li, H., and Liu, Q.A. (2019). Calcium-activated chloride channel A4 (CLCA4) plays inhibitory roles in invasion and migration through suppressing epithelial-mesenchymal transition via PI3K/AKT signaling in colorectal cancer. Med. Sci. Monit. 25, 4176–4185.

Cigic, B., and Pain, R.H. (1999). Location of the binding site for chloride ion activation of cathepsin C. Eur. J. Biochem. 264, 944–951.

Cox, D., Tseng, C.-C., Bjekic, G., and Greenberg, S. (1999). A requirement for phosphatidylinositol 3-kinase in pseudopod extension. J. Biol. Chem. 274, 1240–1247.

Deriy, L.V., Gomez, E.A., Zhang, G., Beacham, D.W., Hopson, J.A., Gallan, A.J., Shevchenko, P.D., Bindokas, V.P., and Nelson, D.J. (2009). Disease-causing mutations in the cystic fibrosis transmembrane conductance regulator determine the functional responses of alveolar macrophages. J. Biol. Chem. 284, 35926–35938.

Di, A., Brown, M.E., Deriy, L.V., Li, C., Szeto, F.L., Chen, Y., Huang, P., Tong, J., Naren, A.P., Bindokas, V., et al. (2006). CFTR regulates phagosome acidification in macrophages and alters bactericidal activity. Nat. Cell Biol. 8, 933–944.

El Chemaly, A., Nunes, P., Jimaja, W., Castelbou, C., and Demaurex, N. (2014). Hv1 proton channels differentially regulate the pH of neutrophil and macrophage phagosomes by sustaining the production of phagosomal ROS that inhibit the delivery of vacuolar ATPases. J. Leukoc. Biol. 95, 827–839.

Flores-Tellez, T.N., Lopez, T.V., Vasquez Garzon, V.R., and Villa-Trevino, S. (2015). Co-expression of ezrin-CLIC5-podocalyxin is associated with migration and invasiveness in hepatocellular carcinoma. PLoS One 10, e0131605.

Grabe, M., Wang, H., and Oster, G. (2000). The mechanochemistry of V-ATPase proton pumps. Biophys. J. 78, 2798–2813.

Gururaja Rao, S., Patel, N.J., and Singh, H. (2020). Intracellular chloride channels: novel biomarkers in diseases. Front. Physiol. 11, 96.

Harl, B., Schmolzer, J., Jakab, M., Ritter, M., and Kerschbaum, H.H. (2013). Chloride channel blockers suppress formation of engulfment pseudopodia in microglial cells. Cell Physiol. Biochem. 31, 319–337.

Hartenstein, V., and Martinez, P. (2019). Phagocytosis in cellular defense and nutrition: a food-centered approach to the evolution of macrophages. Cell Tissue Res. 377, 527–547.

Hernandez-Fernaud, J.R., Ruengeler, E., Casazza, A., Neilson, L.J., Pulleine, E., Santi, A., Ismail, S., Lilla, S., Dhayade, S., MacPherson, I.R., et al. (2017). Secreted CLIC3 drives cancer progression through its glutathione-dependent oxidoreductase activity. Nat. Commun. 8, 14206.

Jankowski, A., Scott, C.C., and Grinstein, S. (2002). Determinants of the phagosomal pH in neutrophils. J. Biol. Chem. 277, 6059–6066.

Jentsch, T.J. (2008). CLC chloride channels and transporters: from genes to protein structure, pathology and physiology. Crit. Rev. Biochem. Mol. Biol. 43, 3–36.

Jiang, L., Salao, K., Li, H., Rybicka, J.M., Yates, R.M., Luo, X.W., Shi, X.X., Kuffner, T., Tsai, V.W., Husaini, Y., et al. (2012). Intracellular chloride channel protein CLIC1 regulates macrophage function through modulation of phagosomal acidification. J. Cell Sci. 125, 5479–5488.

Jovov, B., Ismailov, , II, and Benos, D.J. (1995). Cystic fibrosis transmembrane conductance regulator is required for protein kinase A activation of an outwardly rectified anion channel purified from bovine tracheal epithelia. J. Biol. Chem. 270, 1521–1528.

Kettner, C., Bertl, A., Obermeyer, G., Slayman, C., and Bihler, H. (2003). Electrophysiological analysis of the yeast V-type proton pump: variable coupling ratio and proton shunt. Biophys. J. 85, 3730–3738.

Kim, K.H., Choi, B.K., Song, K.M., Cha, K.W., Kim, Y.H., Lee, H., Han, I.S., and Kwon, B.S. (2013). CRIg signals induce anti-intracellular bacterial phagosome activity in a chloride intracellular channel 3-dependent manner. Eur. J. Immunol. 43, 667–678.

Kissing, S., Saftig, P., and Haas, A. (2018). Vacuolar ATPase in phago(lyso)some biology. Int. J. Med. Microbiol. 308, 58–67.

Kobayashi, T., Zinchuk, V.S., Okada, T., Wakiguchi, H., Kurashige, T., Takatsuji, H., and Seguchi, H. (2000). A simple approach for the analysis of intracellular movement of oxidant-producing intracellular compartments in living human neutrophils. Histochem. Cell Biol. 113, 251–257.

Koncz, C., and Daugirdas, J.T. (1994). Use of MQAE for measurement of intracellular [Cl⁻] in cultured aortic smooth muscle cells. Am. J. Physiol. 267, H2114–H2123.

Landry, D.W., Akabas, M.H., Redhead, C., Edelman, A., Cragoe, E.J., and Alawqati, Q. (1989). Purification and reconstitution of chloride channels from kidney and Trachea. Science 244, 1469–1472.

Littler, D.R., Harrop, S.J., Goodchild, S.C., Phang, J.M., Mynott, A.V., Jiang, L., Valenzuela, S.M., Mazzanti, M., Brown, L.J., Breit, S.N., et al. (2010). The enigma of the CLIC proteins: ion channels, redox proteins, enzymes, scaffolding proteins? FEBS Lett. 584, 2093–2101.

Liu, J., Zhang, D., Li, Y., Chen, W., Ruan, Z., Deng, L., Wang, L., Tian, H., Yiu, A., Fan, C., et al. (2013). Discovery of bufadienolides as a novel class of ClC-3 chloride channel activators with antitumor activities. J. Med. Chem. 56, 5734–5743.

Lymar, S.V., and Hurst, J.K. (1995). Role of compartmentation in promoting toxicity of leukocyte-generated strong oxidants. Chem. Res. Toxicol. 8, 833–840.

Marmagne, A., Vinauger-Douard, M., Monachello, D., de Longevialle, A.F., Charon, C., Allot, M., Rappaport, F., Wollman, F.A., Barbier-Brygoo, H., and Ephritikhine, G. (2007). Two members of the Arabidopsis CLC (chloride channel) family, AtCLCe and AtCLCf, are associated with thylakoid and Golgi membranes, respectively. J. Exp. Bot. 58, 3385–3393.

Monahan, A.J., and Silverman, N. (2017). Relish the thought and channel your chloride, for bacterial clearance depends on it. Cell Host Microbe 21, 657–659.

Moreland, J.G., Davis, A.P., Bailey, G., Nauseef, W.M., and Lamb, F.S. (2006). Anion channels, including ClC-3, are required for normal neutrophil oxidative function, phagocytosis, and transendothelial migration. J. Biol. Chem. 281, 12277–12288.

Nguyen, C.T., Agorio, A., Jossier, M., Depre, S., Thomine, S., and Filleur, S. (2016). Characterization of the chloride channel-like, AtCLCg, involved in chloride tolerance in Arabidopsis thaliana. Plant Cell Physiol. 57, 764–775.

Novarino, G., Fabrizi, C., Tonini, R., Denti, M.A., Malchiodi-Albedi, F., Lauro, G.M., Sacchetti, B., Paradisi, S., Ferroni, A., Curmi, P.M., et al. (2004). Involvement of the intracellular ion channel CLIC1 in microglia-mediated beta-amyloid-induced neurotoxicity. J. Neurosci. 24, 5322–5330.

Olazabal, I.M., Caron, E., May, R.C., Schilling, K., and Machesky, L.M. (2002). Rho-kinase and myosin-II control phagocytic cup formation during CR, but not FcgammaR, phagocytosis. Curr. Biol. 12, 1413–1418.

Peretti, M., Angelini, M., Savalli, N., Florio, T., Yuspa, S.H., and Mazzanti, M. (2015). Chloride channels in cancer: focus on chloride intracellular channel 1 and 4 (CLIC1 AND CLIC4) proteins in tumor development and as novel therapeutic targets. Biochim. Biophys. Acta 1848, 2523–2531.

Pillay, C.S., Elliott, E., and Dennison, C. (2002). Endolysosomal proteolysis and its regulation. Biochem. J. 363, 417–429.

Pong, N.H., Yun, Z., Kejing, S., Hodges, C.A., Drumm, M.L., Guoshun, W., and Charaf, B. (2014). Neutrophil-mediated phagocytic host defense defect in myeloid cftr-inactivated mice. PLoS One 9, e106813.

Redhead, C.R., Edelman, A.E., Brown, D., Landry, D.W., and Alawqati, Q. (1992). A ubiquitous 64-Kda protein is a component of a chloride channel of plasma and intracellular membranes. Proc. Natl. Acad. Sci. U S A 89, 3716–3720.

Rodan, A.R. (2019). Intracellular chloride: a regulator of transepithelial transport in the distal nephron. Curr. Opin. Nephrol. Hypertens. *28*, 360–367.

Rosen, H., Crowley, J.R., and Heinecke, J.W. (2002). Human neutrophils use the myeloperoxidase-hydrogen peroxide-chloride system to chlorinate but not nitrate bacterial proteins during phagocytosis. J. Biol. Chem. *277*, 30463–30468.

Rosen, H., Klebanoff, S.J., Wang, Y., Brot, N., Heinecke, J.W., and Fu, X. (2009). Methionine oxidation contributes to bacterial killing by the myeloperoxidase system of neutrophils. Proc. Natl. Acad. Sci. U S A *106*, 18686–18691.

Saric, A., Hipolito, V.E., Kay, J.G., Canton, J., Antonescu, C.N., and Botelho, R.J. (2016). mTOR controls lysosome tubulation and antigen presentation in macrophages and dendritic cells. Mol. Biol. Cell *27*, 321–333.

Scheel, O., Zdebik, A.A., Lourdel, S., and Jentsch, T.J. (2005). Voltage-dependent electrogenic chloride/proton exchange by endosomal CLC proteins. Nature *436*, 424–427.

Stauber, T., Weinert, S., and Jentsch, T.J. (2012). Cell biology and physiology of CLC chloride channels and transporters. Compr. Physiol. *2*, 1701–1744.

Takano, K., Liu, D., Tarpey, P., Gallant, E., Lam, A., Witham, S., Alexov, E., Chaubey, A., Stevenson, R.E., Schwartz, C.E., et al. (2012). An X-linked channelopathy with cardiomegaly due to a CLIC2 mutation enhancing ryanodine receptor channel activity. Hum. Mol. Genet. *21*, 4497–4507.

Tuxworth, R.I., Weber, I., Wessels, D., Addicks, G.C., Soll, D.R., Gerisch, G., and Titus, M.A. (2001). A role for myosin VII in dynamic cell adhesion. Curr. Biol. *11*, 318–329.

Wang, G. (2016). Chloride flux in phagocytes. Immunol. Rev. *273*, 219–231.

Wang, P., Zeng, Y., Liu, T., Zhang, C., Yu, P.W., Hao, Y.X., Luo, H.X., and Liu, G. (2014). Chloride intracellular channel 1 regulates colon cancer cell migration and invasion through ROS/ERK pathway. World J. Gastroenterol. *20*, 2071–2078.

Wootton, E.C., Dyrynda, E.A., and Ratcliffe, N.A. (2003). Bivalve immunity: comparisons between the marine mussel (Mytilus edulis), the edible cockle (Cerastoderma edule) and the razor-shell (Ensis siliqua). Fish Shellfish Immun. *15*, 195–210.

Zhang, Y.L., Chen, P.X., Guan, W.J., Guo, H.M., Qiu, Z.E., Xu, J.W., Luo, Y.L., Lan, C.F., Xu, J.B., Hao, Y., et al. (2018). Increased intracellular $Cl^{(-)}$ concentration promotes ongoing inflammation in airway epithelium. Mucosal Immunol. *11*, 1149–1157.

Zhao, W., Lu, M., and Zhang, Q. (2015). Chloride intracellular channel 1 regulates migration and invasion in gastric cancer by triggering the ROS-mediated p38 MAPK signaling pathway. Mol. Med. Rep. *12*, 8041–8047.

Supplemental Information

CLIC2α Chloride Channel Orchestrates

Immunomodulation of Hemocyte Phagocytosis

and Bactericidal Activity in *Crassostrea gigas*

Xiangyu Zhang, Fan Mao, Nai-Kei Wong, Yongbo Bao, Yue Lin, Kunna Liu, Jun Li, Zhiming Xiang, Haitao Ma, Shu Xiao, Yang Zhang, and Ziniu Yu
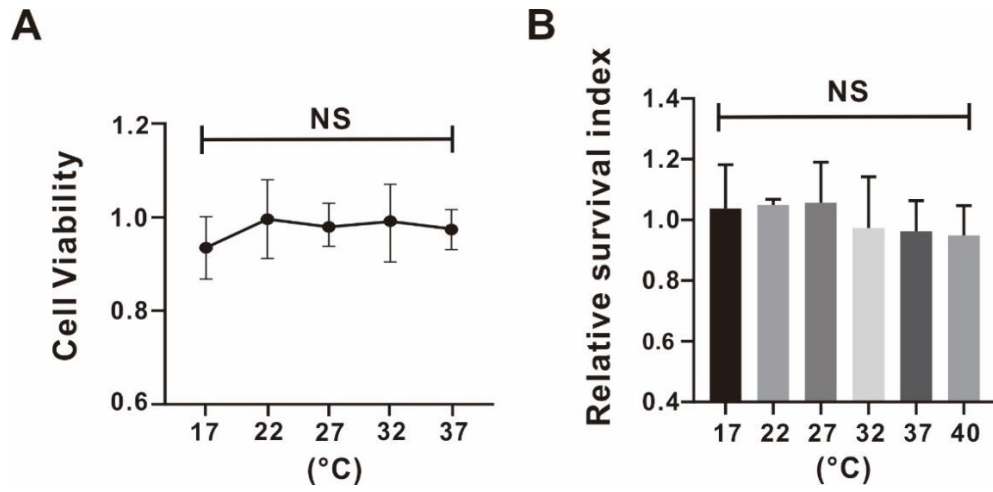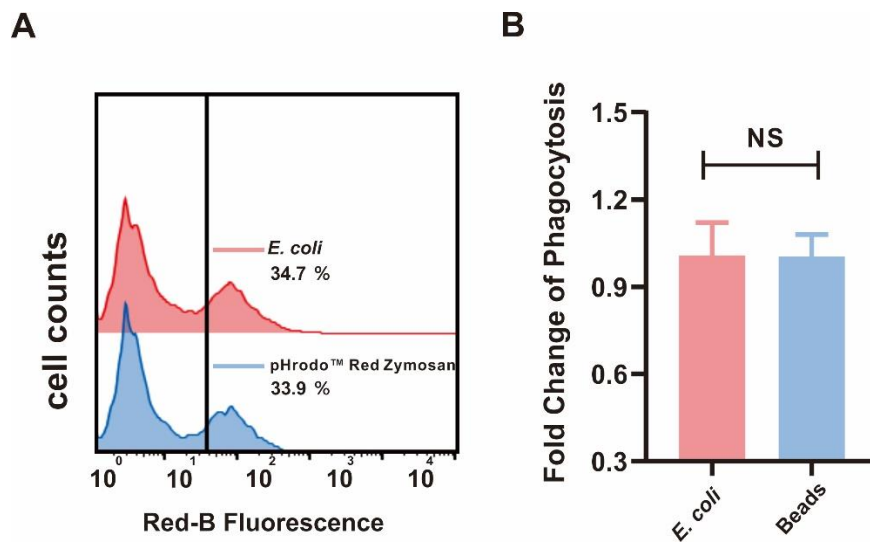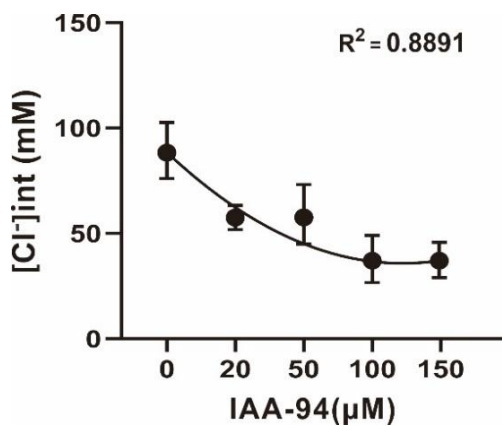
Figure S1.

Figure S2.

Figure S3.

Figure S4.
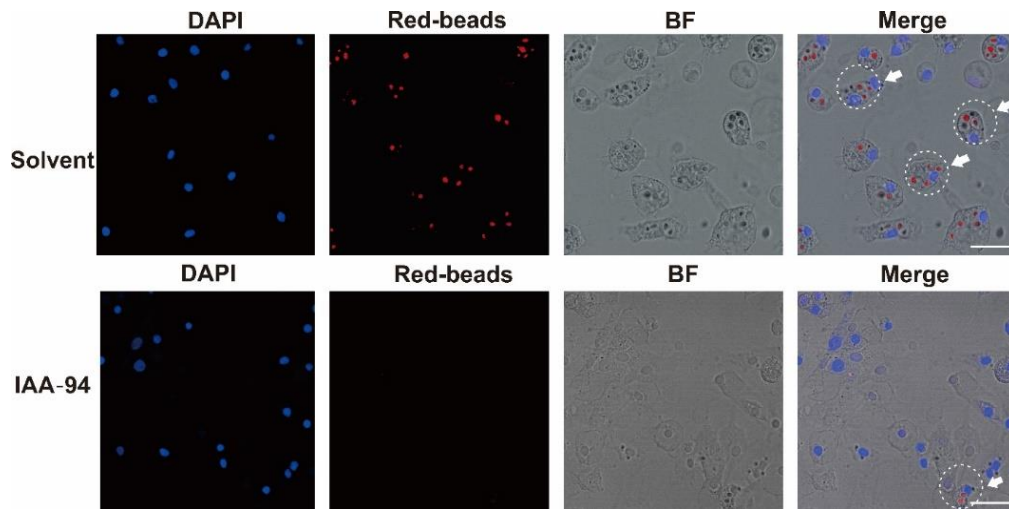
Figure S5.
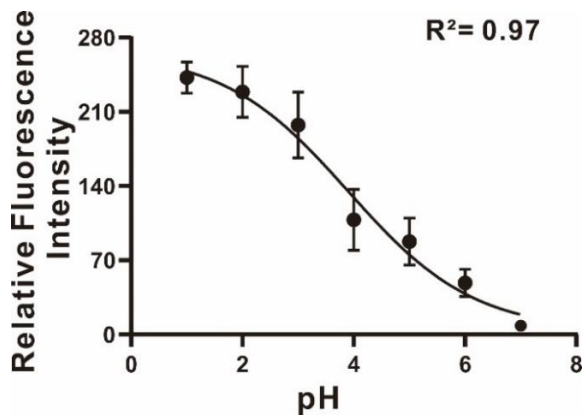
Figure S6.

Figure S7.

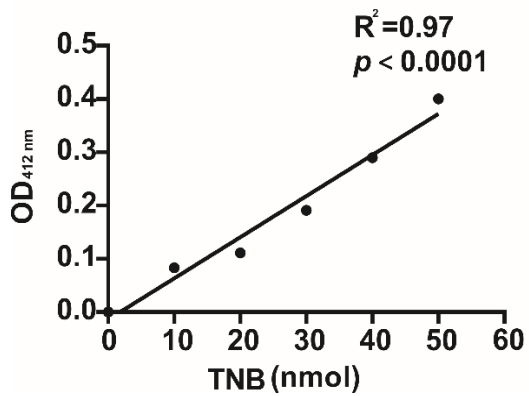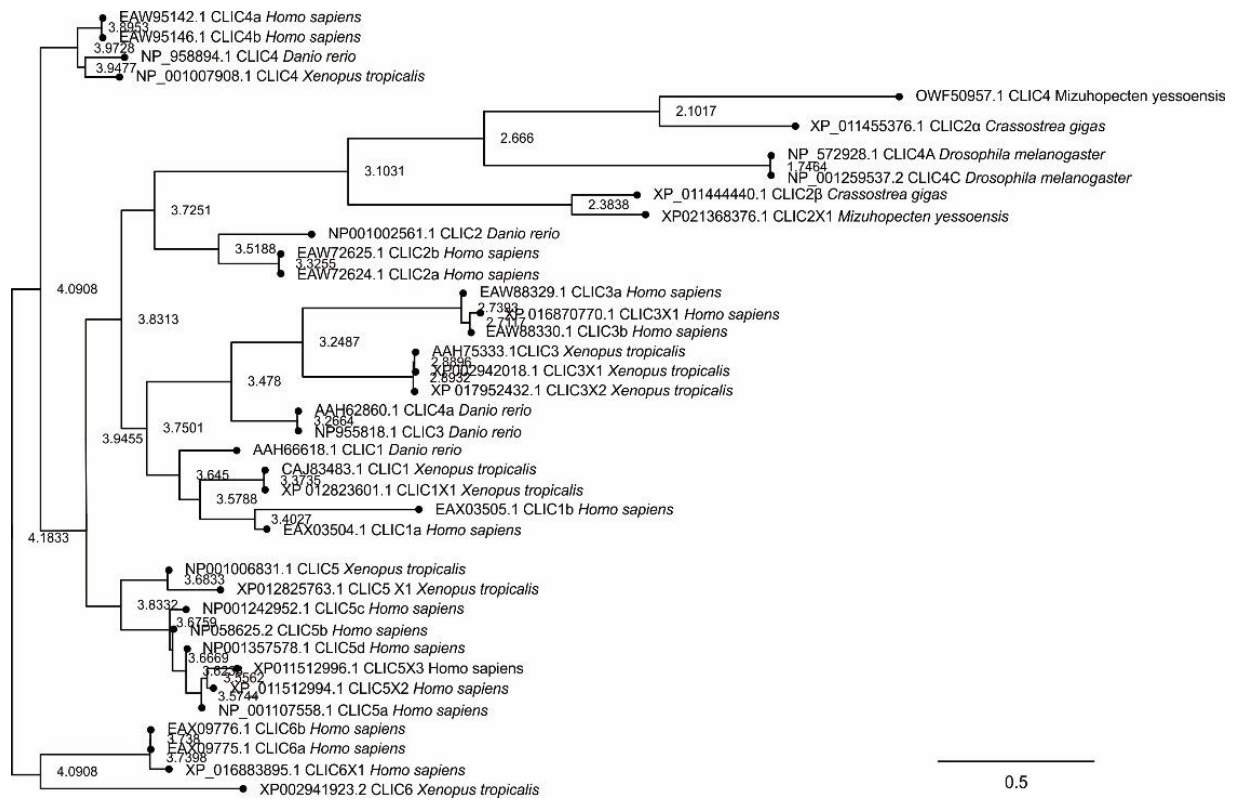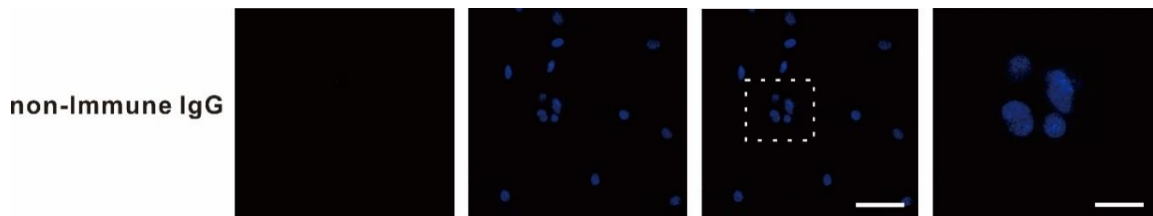**Figure S8.**

<u>**Supplemental Figure Legends**</u>

Figure S1. Cell viability tests of oyster hemocytes during 2 h of *in vitro* primary culture, related to Figure 1. A, Cells viability was assessed by measurement intracellular ATP levels. B, Relative cell survival rates were measured by Trypan blue staining. Statistical analysis was done by one-way ANOVA followed by Tukey's *post hoc* test; NS: no significant difference, all data are presented as mean ± S.D. (n = 3).

Figure S2. Flow cytometry analysis was conducted to measure the rate of phagocytosis, related to Figure 1. A, Red color and blue color represent groups phagocytosing *E. coli* and pHrodo™ Red zymosan, respectively. B, Data analysis was performed by using GraphPad Prism 7 software. n = 3; data were analyzed by unpaired t test, and asterisks in the graphs

indicate *p* values of significance; NS: no significant difference; data are presented as mean ± S.D.

Figure S3. Dose-dependent response curve for IAA-94 effects on chloride flux in oyster hemocytes after bacterial challenge, related to Figure 2. IAA-94 is a potent indanyloxyacetic acid blocker of epithelial chloride channels. All data are presented as mean ± S.D. (*n* = 3).

Figure S4. Dysphagocytosis in phagosomes following particles ingestion in oyster hemocytes treated with IAA-94, related to Figure 2. Arrows refer to cells that have engulfed the beads.

Figure S5. Analysis on the relationship between fluorescence intensity and pH of pHrodo™ Red zymosan, related to Figure 4. All data are presented as mean ± S.D. (*n* = 3).

Figure S6. Standard curve for TNB (measure of production of hypochlorous acid) and optical density, related to Figure 4.

Figure S7. CLIC superfamily protein sequences from different species including *Homo sapiens, Mizuhopecten yessoensis, Xenopus tropicalis, Danio rerio, Drosophila melanogaster and Crassostrea gigas*, related to Figure 5. Protein sequence accession numbers are as shown at the end of branch name.

Figure S8. Negative controls for subcellular localization of CLIC2α, related to Figure 5. Negative control groups are stained with non-immune IgG. Nuclei (blue) were counterstained with DAPI. Scale bar: 5 μm. Insets show higher magnifications. Scale bar of insets: 3 μm.

Supplemental Table

Table S1. Summary of primers used in this work, related to Figure 6 and Figure 7.

Names	Sequences (5'-3')
DsRNA templates amplification	
DsCLIC2α-F	TAATACGACTCACTATAGGTCCCAGTAGTGATTGGAACGAG
DsCLIC2α-R	TAATACGACTCACTATAGGCCCTGTATTGCTCTCCTGCC
DsGFP-F	GGATCCTAATACGACTCACTATAGGACAAGTTCAGCGTGTCCG
DsGFP-R	GGATCCTAATACGACTCACTATAGGTTCACCTTGATGCCGTTC
Quantitative RT-PCR (qRT-PCR)	
Q-CLIC2α-F	TATGGAACGTGGATACCAGACAA
Q-CLIC2α-R	CCGTTTGACCCTTCACCATC
Q-GAPDH-F	GGATTGGCGTGGTGGTAGAG
Q-GAPDH-R	GTATGATGCCCCTTTGTTGAGTC

Transparent Methods

Animals, pathogen challenge and hemolymph preparation

Crassostrea gigas (2 years old) were obtained from the Marine Biology Research Station at Zhanjiang of the Chinese Academy of Sciences (Zhanjiang, Guangdong, China). For acclimation, oysters were maintained at 27±1°C in tanks with re-circulating seawater for one month before experiments. Oysters were fed twice daily with *Tetraselmis suecica* and *Isochrysis galbana*. All animal experiments were conducted in accordance with the guidelines and approval of Animal Research and Ethics Committees of the Chinese Academy of Sciences.

For bacterial challenge, *Vibrio parahaemolyticus* was cultured in LB (Luria-Bertani) broth at 37°C to a turbidity of OD_{600nm} = 0.6-0.8, and then centrifuged at 800×g for 10 min at 4°C. After being washed for 3 time in PBS (PBS, 0.14 M sodium chloride, 3 mM potassium chloride, 8 mM disodium hydrogenphosphate dodecahydrate, 1.5 mM potassium phosphate monobasic, pH 7.4), bacterial pellet was resuspended in PBS to an adjusted density of OD_{600nm} = 1.0. Oysters in the challenged group were injected with a 100-μL suspension into the adductor muscle, while oysters in the control group were injected with an equal volume of PBS. After injection, oysters were returned to separate tanks for subsequent incubation or sampling.

Hemolymph was drawn from the posterior adductor muscle of *C. gigas* by using a sterile 1-mL syringe. Hemolymph was kept and immediately centrifuged at 200×g for 10 min to collect hemocytes, then the supernatant was sterilized through a 0.22 μM filter (Sangon Biotech, F513134). Hemocytes were incubated in each petri dish with hemolymph serum at 27°C for subsequent analyses.

Cell viability test

Approximately $1×10^6$ cells were cultured in 12-well plates with filtered plasma and incubated at different temperatures. CellTiter-Lumi™ Luminescent Cell Viability Assay Kit (Promega, USA) was used to quantify ATP content, which is one marker for living cells. According to the manufacturer's protocol (Beyotime, C0065S), treated hemocytes were equilibrated at room temperature for 10 min for the next operation. 50 μL CellTiter-Lumi ™ luminescence detection reagent was added to each well of a 96-well microplate. The 96-well microplate was gently shaken at room temperature for 2 min to promote cell lysis. Lysed cells were incubated at room temperature (about 27°C) for 10 min to stabilize luminescence signals. A multi-functional microplate reader was used for chemiluminescence detection of samples. Relative viability of cells was directly calculated based on chemiluminescence readings.

In Trypan blue staining assay, hemocytes were stained with a standard Trypan blue solution (0.04% in PBS) for 5 min. Cells were enumerated under a light microscope with a hemocytometer, where blue-colored cells were considered to be dead. All experiments were performed in at least triplicates.

Determination of $[Cl^-]_i$

This part of the study was conducted as previously described with slightly modification

(Zhang et al., 2018). Briefly, levels of intracellular Cl⁻ concentration ($[Cl^-]_i$) were measured by using the Cl⁻ specific fluorescent probe MQAE (5 mM, Beyotime, S1082), a selective chloride ion indicator. Upon binding halide ions such as chloride, MQAE fluorescence is quenched, resulting in a decrease in fluorescence intensity without a shift in wavelength (Ikeuchi et al., 2018).300 μL of hemocytes were cultured in glass bottom dishes at 27°C for 15 min. At the end of appropriate treatments, oyster hemocytes were washed twice with Cl⁻-free Tyrode solution (NaCl was replaced by equimolar amounts of D-glucuronic acid; $MgCl_2$ by $MgSO_4$; KCl by potassium gluconate), and loaded with 10 mM of MQAE in dark at 27°C for 30 min Thereafter, samples were rinsed 3 times with Cl⁻-free Tyrode solution. To calibrate the probe's fluorescence intensities relative to $[Cl^-]_i$, standard Tyrode solutions are configured and delivered as described. Different predetermined concentrations of Cl⁻ (20, 40, 60, 80 and 100 mM) were prepared with the solutions which, where appropriate, also contained tributyltin chloride (10 μM, J&K Scientific, T773810), nigericin (10 μM, MedChemExpree, HY-127019) and valinomycin (10 μM, MedChemExpree, HY-N6693) to disrupt membrane channel activities and allow equilibration of intracellular Cl⁻ with that of an extracellular buffer. Then, a calibration curve was constructed by fitting fluorescence intensities onto corresponding Cl⁻ concentrations, and $[Cl^-]_i$ could be calculated based on the calibration curve.

For other experiment, the oyster hemocytes were cultured with filtered plasma, and loaded with 10 mM of MQAE in dark at 27°C for 30 min for florescence detection. IAA-94 (100 μM, MedChemExpree, HY-12693), a cell permeable chloride ion channel blocker, or DMSO (vehicle) was treated to determine changes in $[Cl^-]_i$ during phagocytosis in oyster hemocytes.

Phagocytosis assay

E. coli transformed with an indicator plasmid (pFPV25.1) expressing RFP (red fluorescent protein) was cultured to a turbidity of OD_{600nm} = 0.6-0.8 at 37°C. Then, the bacterium was washed 3 times in PBS (0.14 M sodium chloride, 3 mM potassium chloride, 8 mM disodium hydrogenphosphate dodecahydrate, 1.5 mM potassium phosphate monobasic, pH 7.4) and resuspended to a final density of 1.0×10^7 CFU per mL for subsequent phagocytosis assays (Duperthuy et al., 2011; Wang et al., 2014). Hemocytes cultured in a 24 well plate and the determined reagent were included in the buffer to incubate the cells for 30 minutes at room temperature and washed 3 times with PBS. Next, hemocytes were incubated with the prepared bacteria for 15 min at a MOI (multiplicity of infection) of 50. Cell were washed with Tris buffer (pH 8.0, 50 mM, Sangon Biotech, A610195) for 3 times to remove unbound bacteria and then suspended in PBS supplemented with 1.5‰ EDTA. Trypan blue was used to inhibit further attachment of hemocytes to bacteria (Guckian et al., 1978). Finally, flow cytometry analysis by Guava® easyCyte™ was performed to quantify phagocytosis in oyster hemocytes. Cells taking up *E. coli* were recognized by RFP reporter fluorescence, which provided an indication of uptake capacity (proportional to the number of bacteria retained). Phagocytosis by hemocytes was monitored with at least a total of 10,000 events. Data were analyzed with the FlowJo

software (version V10).

Bacterial clearance assay

This assay was performed as described previously with minor modifications (Saleh et al., 2006). For the experiments, two strains of bacteria, *Escherichia coli* (DH5α) and *V.parahaemolyticus* (ZJ51) (of a working density at $OD_{600nm} = 0.2$), were cultured at 37°C. After incubation, bacteria were harvested by centrifugation at low speed, followed by washing 3 times with Tris buffer (50 mM, pH 8.0, Sangon Biotech, A610195) and resuspension in 1 ml PBS for subsequent assays. Approximately 2×10^5 hemocytes per well was cultured in a 24-well plate and subsequently challenged with preprocessed bacteria at an MOI (multiplicity of infection) of 50 at room temperature. Cells were then briefly treated with 0.02% trypsin-EDTA for 4 times to remove extracellular bacteria. Subsequently, IAA-94 (100 μM) and DMSO (vehicle) were added to the filtered body fluids (except for the knockdown group) to pretreat cells for 30 min. After 30 min to kill the internalized bacteria, hemocytes were lysed in 1 mL PBS containing 0.05% Triton X-100. Finally, 100 μL of the lysate was used as an inoculum on LB agar plates for enumerating bacterial colonies. For each group, three wells were used to perform the bacterial clearance assay and each experiment was independently repeated 3 times.

Western blot analysis

Hemocytes were collected and each sample was analyzed in triplicates. Specifically, hemocytes were harvested and lysed in IP buffer supplemented with a protease and phosphatase inhibitor cocktail according to the manufacturer's protocol (Sangon Biotech, C50035). Lysates were centrifuged at 1,200×g for 20 min at 4°C, and supernatant was diluted 10 times to determine protein concentrations by using the bicinchoninic acid (BCA) protein assay (ThermoFisher Scientific, 23227). Samples containing equal amounts of proteins per lane were resolved by sodium dodecyl sulfate-polyacrylamide gel electrophoresis (SDS-PAGE) and then transferred to 0.2 μm polyvinylidene difluoride membranes (Merck Millipore, ISEQ00010). The membranes were blocked with QuickBlock™ blocking buffer for Western blotting (Beyotime, P0252), and then incubated with appropriate primary antibodies overnight at 4°C. The membranes were washed with PBST (phosphate buffered solution with 0.1% Twen-20 [Damao, 9005-65-6]), and then incubated for 2 h at room temperature with a secondary antibody. All primary and secondary antibodies used were diluted by a ratio of 1:1000 and 1:2000, respectively, in QuickBlock™ blocking buffer. The protein bands of interest were visualized by using an ECL luminescence reagent (Sangon Biotech, C510043). Relative expression of protein was quantified by using ImageJ software (version 1.8.0).

The following antibodies were used to detect their corresponding protein substrates: rabbit anti-Akt (Cell Signaling Technology, C67E7), rabbit anti-phospho-Akt (Thr308) (Cell Signaling Technology, 244F9), rabbit anti-*β*-actin (Cell Signaling Technology, 8457), anti-rabbit HRP-linked secondary antibody (Cell Signaling Technology, 7074).

Determination of phagosomal acidification index

Freshly harvested hemocytes were incubated in 35-mm diameter glass-bottom dishes (NEST, 801001) for 30 min at 27°C with pHrodo™ Red zymosan (Thermo Fisher Scientific, P35364). Excess zymosan was removed by washing cells 3 times with PBS. Cells were then fixed by with cold 4% paraformaldehyde for 10 min. Afterwards, nuclei were stained with DAPI (Sigma, 1.5 μg/mL) and washed 3 times with PBS. Hemocytes were bathed in 200 μL PBS and visualized under a Leica SP8 confocal microscope.

RNA interference (RNAi)

To clarify the functional relevance of CLIC2α in oyster hemocytes, CLIC2α gene was knocked down *in vivo* via dsRNA-mediated RNA interference. The primers used to synthesize dsRNA are as shown in Table S1. A CLIC2α cDNA fragment and a GFP cDNA fragment (negative control) were amplified with primer pairs with T7 promoter overhangs (Promega, RiboMAX™ Express RNAi System). PCR products thus resulted were used as templates to synthesize dsRNA according to the manufacturer's instructions. Ten oysters were randomly assigned into 2 groups and placed in 2 tanks: the treatment and control groups. Each oyster was injected with 50 μg dsRNA and three individuals from each group were chosen randomly for the collection of hemocytes. Phagocytosis rate, bacterial clearance rate and degree of phagosomal acidification were evaluated 3 days after dsRNA injection. The expression level of CLIC2α was then determined by RT-qPCR and Western blot.

Total RNA extraction and quantitative real-time PCR analysis

Hemocytes were collected as above and total RNA was isolated with TRIzol Reagent (Invitrogen, 15596-026) according to the manufacturer's protocol. The RNA quality and quantity were detected using NanoDrop 2000C (Thermo Fisher Scientific, USA). Extracted RNA was converted to cDNA with the PrimerScript™ first strand cDNA synthesis kit (TAKARA, RR047A), then subjected to quantification analysis by using the 2×RealStar Green Power mixture (GenStar, A311) and LightCycler® 480 II (Roche, Switzerland) according to manufacturer's protocol. Primers were designed with Primer Premier (v5.0), and their sequences are as listed in Table S1. All experiments were performed in triplicates by using GAPDH mRNA as an internal control. Analysis of the dissociation curve of the amplification products was constructed to confirm specificity at the end of each PCR. Relative gene expression was calculated by using the $2^{-\Delta\Delta Ct}$ method. Data was represented by using SPSS10.0 statistical software, and significance between two groups was determined by Student's *t*-test.

Determination of phagosomal-lysosomal fusion

Hemocytes were cultured in 35-mm diameter glass-bottom dishes (NEST, 801001) and then incubated with 100 μM IAA-94 and the same dose of DMSO (solvent) for 30 min. Cells were then washed 3 times with PBS and further incubated with AlexaFluor-488-conjugated zymosan for an additional 20 min. Excess zymosan is removed by washing with PBS for 3 times. As per the manufacturer's protocol, cells were incubated with Lyso-Tracker Red (50 nM, Beyotime, C1046), a lysosomal red fluorescent probe for 30 min at room temperature in dark.

Subsequently, cells were fixed with cold 4% paraformaldehyde and their nuclei were stained with DAPI (Sigma, 1.5 µg/mL) as mentioned above. Imaging data were collected by using a Leica SP8 confocal microscope. Upon fusion, phagosomes (intracellular zymosan, green) co-localizing with lysosomes (red) appeared yellow.

Determination of HOCl levels *in vivo*

Hypochlorous acid (HOCl) levels in the samples were measured by a colorimetric MPO activity assay kit (Sigma, MAK068) according to the manufacturer's instructions. MPO (myeloperoxidase) catalyzes the formation of HOCl, which reacts with endogenous taurine to form taurine chloroamine. Taurine chloroamine reacts with the chromophore TNB, resulting in the formation of a colorless product, DTNB. Yields of this reaction can be approximately defined as the amount of taurine chloramine consuming the chromophore TNB. In brief, hemocytes after *in vivo* bacterial challenge were collected from oysters and homogenized in 4 equivalent volumes of MPO assay buffer. Among them, we used flow cytometry to ensure consistency of the number of sampled hemocytes. Then, hemocytes were centrifuged at 13,000×g for 10 min at 4°C to remove insoluble materials. Five microliters of the samples from supernatant (MPO substrate) were loaded into a 96-well microplate to incubate with MPO assay buffer at room temperature for 1 h, shielded from light. Then, 2 µL of a stop mix was added to the wells, followed by incubation for 10 min. Next, 50 µL of the TNB reagent/standard was added to the samples which were left to stand for an additional 10 min. Subsequently, absorbance at 412nm (A_{412}) was detected by means of an EnSightTM multimode plate reader (PerkinElmer, USA). Numerical data were obtained by comparing absorbance measurements against the standard curve.

ORF cloning and bioinformatics analysis

Partial cDNA sequence of *C. gigas* was BLAST searched in the oyster genome library (http://blast.ncbi.nlm.nih.gov/Blast.cgi). Based on identified sequences, the ORF of the CLIC2α genes were obtained by polymerase chain reaction (PCR), according to the manufacturer's instructions (GenStar, A012-01). Deduced amino acid sequences were obtained with the aid of ORF Finder (http://www.ncbi.nlm.nih.gov/gorf/orfig.cgi). A phylogenetic tree was constructed based on amino acid sequences of known CLICs proteins by performing Bayesian phylogenetic analysis. Further, transmembrane results were predicted with MemBrain (http://www.csbio.sjtu.edu.cn/bioinf/MemBrain).

Antibody production

The two amino acid sequences 1-129 a.a. and 201-292 a.a. in the ORF protein of CLIC2α were selected for protein expression and purification as antigens in mixed immunization. White rabbits are used as experimental animals for immunization. Multiple injections of a total amount of 600 µg of antigens and complete Freund's adjuvant were injected subcutaneously on the back of the rabbit. Injection proceeded once every two weeks, followed by evaluation of serum titers after four injections. Pre-sera were used as a negative control for antibody titer testing.

Rabbits were bled after passing the test. Then, protein Affinity purification, HABP affinity purification, and antigen affinity purification were performed successively to purify desired sera. The resultant purified antibodies were validated in immunoblotting and stored for subsequent experiments.

Immunofluorescence preparation

For imaging, hemocytes were fixed with cold 4% paraformaldehyde for 10 min, rinsed 3 times in PBS and permeabilized with 0.05% Triton in PBS for 15 min at room temperature. Then, hemocytes were blocked with QuickBlock™ blocking buffer (Beyotime, P0252) for 60 min, incubated overnight with appropriate primary antibodies at 4°C. CLIC2α was stained with an affinity purified rabbit polyclonal antibody (Sinobiological). After washing off primary antibodies, specimens were incubated in a fluorochrome-conjugated secondary antibody (Cell Signaling Technology, #4414) diluted in antibody dilution buffer for 1 h at room temperature in dark. DAPI staining was done to counterstain nuclei (Sigma, 1.5 μg/mL), followed by washing in PBS for 3 times. The hemocyte samples thus prepared were then immersed in 200 μL PBS and visualized under a Leica SP8 confocal microscope.

Confocal microscopy

Variations in Cl⁻ levels were monitored by using the fluorescent dye *N*-(ethoxycarbonylmethyl)-6-methoxyquinolinium bromide (MQAE, 5 mM, Beyotime, S1082), whose fluorescence becomes quenched via collision with chloride in oyster hemocytes. Experimentally, cells were allowed to engulf red-emission zymosan and fluorescent *E. coli* for a 30-min period to ensure that the majority of the immunostimulants have entered the phagosomal compartment. Fluorescence micrographs were acquired by using a Leica SP8 confocal fluorescence laser scanning system (Leica Microsystems, Germany). Lasers were used at the following excitation/emission parameters: λ_{ex} 405 nm for MQAE (λ_{em} 460 nm), λ_{ex} 560 nm for pHrodo™ Red zymosan (λ_{em} 585 nm), λ_{ex} 405 nm for DAPI (λ_{em} 454 nm), λ_{ex} 577 nm for Lyso-Tracker Red (λ_{em} 590 nm) and λ_{ex} 555 nm for RFP (λ_{em} 584 nm). Series of optical sections were collected and processed by using Image-Pro Plus 6.0. For analysis of imaging data, the bright field and fluorescence channels of representative images were superimposed to confirm cell morphological features and phagocytosis events. Each image regions of interest (ROIs) was selected in Image Pro Plus, corresponding to individual phagocytosis events or whole cells subjected to a particular treatment. To avoid bias, all individuals in the recording optical field were processed for data analysis except for: (1) cells with marked morphological alterations; or (2) aggregating cells. Typically, up to 5-20% of such visually deviant cells may be excluded from analysis (Jiang et al., 2012).

Statistical analysis

Data processing and statistical analyses were performed by using GraphPad Prism (version 8.0.1). All statistical values were expressed as the mean ± S.D., with the number of experiments (*n*) in parentheses. Significance between groups was determined by Student's *t*-

test, while comparisons for more than two groups were done by one-way ANOVA followed by Tukey's *post hoc* test with SPSS (version 22.0). Asterisks indicate a significance difference of $p < 0.05$.

Supplemental References

Duperthuy, M., Schmitt, P., Garzon, E., Caro, A., Rosa, R.D., Le Roux, F., Lautredou-Audouy, N., Got, P., Romestand, B., de Lorgeril, J*., et al.* (2011). Use of OmpU porins for attachment and invasion of Crassostrea gigas immune cells by the oyster pathogen Vibrio splendidus. Proc Natl Acad Sci U S A *108*, 2993-2998.

Guckian, J.C., Christensen, W.D., and Fine, D.P. (1978). Trypan blue inhibits complement-mediated phagocytosis by human polymorphonuclear leukocytes. J Immunol *120*, 1580-1586.

Ikeuchi, Y., Kogiso, H., Hosogi, S., Tanaka, S., Shimamoto, C., Inui, T., Nakahari, T., and Marunaka, Y. (2018). Measurement of [Cl(-)]i unaffected by the cell volume change using MQAE-based two-photon microscopy in airway ciliary cells of mice. J Physiol Sci *68*, 191-199.

Jiang, L., Salao, K., Li, H., Rybicka, J.M., Yates, R.M., Luo, X.W., Shi, X.X., Kuffner, T., Tsai, V.W., Husaini, Y*., et al.* (2012). Intracellular chloride channel protein CLIC1 regulates macrophage function through modulation of phagosomal acidification. J Cell Sci *125*, 5479-5488.

Saleh, M., Mathison, J.C., Wolinski, M.K., Bensinger, S.J., Fitzgerald, P., Droin, N., Ulevitch, R.J., Green, D.R., and Nicholson, D.W. (2006). Enhanced bacterial clearance and sepsis resistance in caspase-12-deficient mice. Nature *440*, 1064-1068.

Wang, X.W., Zhao, X.F., and Wang, J.X. (2014). C-type lectin binds to beta-integrin to promote hemocytic phagocytosis in an invertebrate. J Biol Chem *289*, 2405-2414.

Zhang, Y.L., Chen, P.X., Guan, W.J., Guo, H.M., Qiu, Z.E., Xu, J.W., Luo, Y.L., Lan, C.F., Xu, J.B., Hao, Y*., et al.* (2018). Increased intracellular Cl(-) concentration promotes ongoing inflammation in airway epithelium. Mucosal Immunol *11*, 1149-1157.